

OFFICE OF CIVILIAN RADIOACTIVE WASTE MANAGEMENT
SPECIAL INSTRUCTION SHEET

1. QA: QA
Page: 1 of 1

Complete Only Applicable Items

This is a placeholder page for records that cannot be scanned.

2. Record Date 09/28/2001	3. Accession Number <i>MOL.20011017.0091</i>
4. Author Name(s) SUSAN LESTRANGE	5. Author Organization N/A
6. Title/Description GEOCHEMISTRY MODEL VALIDATION REPORT: MATERIAL DEGRADATION AND RELEASE MODEL	
7. Document Number(s) ANL-EBS-GS-000001	8. Version Designator REV. 00
9. Document Type REPORT	10. Medium OPTIC/PAPER
11. Access Control Code PUB	
12. Traceability Designator DC# 28774	
13. Comments THIS IS A ONE-OF-A-KIND DOCUMENT DUE TO THE COLORED GRAPHS ENCLOSED AND CAN BE LOCATED THROUGH THE RPC.	

OFFICE OF CIVILIAN RADIOACTIVE WASTE MANAGEMENT

MOL.20011017.0091

ANALYSIS/MODEL COVER SHEET

1. QA: QA

Complete Only Applicable Items

Page: 1 of 66

2. <input type="checkbox"/> Analysis		Check all that apply	
Type of Analysis	<input type="checkbox"/> Engineering <input type="checkbox"/> Performance Assessment <input type="checkbox"/> Scientific		
Intended Use of Analysis	<input type="checkbox"/> Input to Calculation <input type="checkbox"/> Input to another Analysis or Model <input type="checkbox"/> Input to Technical Document <input type="checkbox"/> Input to other Technical Products		
Describe use:			
3. <input checked="" type="checkbox"/> Model		Check all that apply	
Type of Model	<input type="checkbox"/> Conceptual Model <input type="checkbox"/> Mathematical Model <input checked="" type="checkbox"/> Process Model		
Intended Use of Model	<input checked="" type="checkbox"/> Input to Calculation <input checked="" type="checkbox"/> Input to another Model or Analysis <input checked="" type="checkbox"/> Input to Technical Document <input checked="" type="checkbox"/> Input to other Technical Products		
Describe use:			
To predict the degradation and release of radionuclides from a degrading waste package.			

4. Title:

Geochemistry Model Validation Report: Material Degradation and Release Model

5. Document Identifier (including Rev. No. and Change No., if applicable):

ANL-EBS-GS-000001 REV 00

6. Total Attachments:

Three

7. Attachment Numbers - No. of Pages in Each:

I (CD-ROM), II(5), III(2)

	Printed Name	Signature	Date
8. Originator	Harlan Stockman, Kaveh Zarrabi, Emma Parker, and Susan LeStrange	Susan LeStrange	9/28/01
9. Checker	Paul Domski (technical) Kristine Dutton (compliance)	Paul Domski (FOR PAUL DOMSKI) Kristine Dutton	9/28/01 9/28/01
10. Lead/Supervisor	Susan LeStrange	Susan LeStrange	9/28/01
11. Responsible Manager	Daniel Thomas	Daniel Thomas	09/28/2001

12. Remarks:

CONTENTS

	Page
Acronyms and Abbreviations	7
1. Purpose.....	8
2. Quality Assurance	9
3. Computer Software and Model Usage	10
3.1 Software	10
3.2 Models.....	11
4. Inputs.....	11
4.1 Data and Parameters.....	11
4.1.1 Densities and Molecular Weights of Solids	11
4.1.2 Thermodynamic Database	13
4.2 Criteria	13
4.3 Codes and Standards	13
5. Assumptions.....	14
6. Model	18
6.1 Conceptual Model.....	18
6.2 Model Implementation.....	18
6.2.1 Step-By-Step Model Description	18
6.2.2 Incoming Water Composition	29
6.2.3 Drip Rate of Incoming Water	30
6.2.4 Sequence of Degradation Scenarios	30
6.2.5 Suppressed Minerals.....	31
6.2.6 Consequences of Lowered fO ₂	31
6.3 Model Validation	33
6.3.1 Glass Degradation Sub-Model	33
6.3.1.1 Metrics for Validation.....	34
6.3.1.2 Methods: MCC-4 Models.....	35
6.3.1.3 Results: MCC-4 Models	37
6.3.1.4 Methods: Archeological Models.....	41
6.3.1.5 Results: Archeological Models.....	43
6.3.2 Summary of Glass Modeling.....	44
6.3.3 Fuel Degradation Sub-Model	46
6.3.3.1 Preliminary Fuel Model 1 and PuO ₂ Solubility Sensitivity	46
6.3.3.2 Degradation Fuel Model 2	48
6.3.4 Solubility-Limiting Uranium Phases in Mixed Glass/Fuel Systems	52
6.3.4.1 EQ6 File Inputs.....	53
6.3.4.2 Method.....	54
6.3.4.3 Summary	57

CONTENTS (Continued)

	Page
7. Conclusions	58
8. Inputs and References	60
9. Attachments.....	66

FIGURES

	Page
6-1: Case s5: Uranium Enrichment Fraction and Total Aqueous U and Pu	29
6-2: Aqueous U and Pu concentrations in the WP	32
6-3: Molal Na vs Time for Analytical Solution vs Model	37
6-4: Predicted Si, K, Ca and Na Variations for MCC-4	38
6-5: Predicted pH Variations for MCC-4	39
6-6: Corrosion Minerals Predicted for MCC-4 Model A	40
6-7: Corrosion Minerals Predicted for MCC-4 Model C2	40
6-8: Experimentally Observed (error bar) Aqueous Mg Concentrations, and Concentrations Predicted for Models C1, C2 and C3	41
6-9: Geometry for Archeological Glass Corrosion Models I and II	42
6-10: pH and Glass Consumption for In-Soil Corrosion Model, Model I	43
6-11: pH and Glass Consumption for In-Soil Corrosion Model, Flow Rate Dropped by 10x, Model II	44
6-12: Minerals Predicted for In-Soil Corrosion Model, Model I	45
6-13: Minerals Predicted for In-Soil Corrosion Model, Flow Rate Dropped by 10x, Model II	45
6-14. Simulated Versus Experimental Pu Concentration	47
6-15: Fuel Model 2A. Concentration of Radionuclide Elements and Minerals vs. Time	50
6-16: Fuel Model 2A. Moles of Minerals and Aqueous Concentrations of Pu and U vs. Time....	50
6-17: Uranium Concentration Measured in 0.4 μm Filtered Solution Sample (Wilson, Figure 2)	51
6-18: Fuel Model 2B, Moles of Minerals and Aqueous Concentrations of Pu and U vs. Time....	52
6-19: EQ6 Run with no Si Minerals Suppressed	55
6-20: EQ6 Run with Chalcedony Suppressed	55
6-21: EQ6 Run with Chalcedony, Cristobalite (alpha) & (beta), and Coesite Suppressed	56

FIGURES (Continued)

	Page
6-22: EQ6 Run with All Five Si Minerals Suppressed.....	56
6-23: EQ6 Run with Weeksite Forming, Run out to 300,000 years	57

TABLES

	Page
3-1: Computer Software Used in the Model	10
4-1. Densities, Molecular Weights and Molar Volumes of Precipitated Solids	12
6-1: Steel Compositions, Densities, and Degradation Rates.....	21
6-2. Simplified Glass Composition, Density, and Degradation Rates.....	22
6-3. Composition and Degradation Rates of Pu-ceramic.....	23
6-4. Drip Rate Values for Input to EQ6.....	23
6-5. EQ6 Input File Elemental Molal Composition for J-13 Well Water.....	24
6-6. Summary of Single-Stage EQ6 Cases for Pu-Ceramic Waste Package	25
6-7. Summary of Multiple-Stage EQ6 Cases for Pu-Ceramic Waste Package.....	26
6-8. Result of Sensitivity Analyses.....	27
6-9. Composition of Corrosion Products ^b (grams) and Density in Selected Years for Case s10 (p52_L142)	28
6-10: Simplified GICI Glass Composition	35
6-11. Comparison of Results with Reduced PuO ₂ LogK Values.....	48
6-12: Sorption Coefficient Distributions for UZ Unite.....	51
6-13. Properties of Reactants	53
6-14. EQ6 Input File Elemental Molal Composition for J-13 Well Water.....	54

ACRONYMS AND ABBREVIATIONS

AMR	Analysis and Modeling Report
CD-ROM	Compact Disc - Read Only Memory
CRWMS	Civilian Radioactive Waste Management System
CSNF	Commercial Spent Nuclear Fuel
DHLW	Defense High Level Waste
DOE	U.S. Department of Energy
DTN	Data Tracking Number
EDX	Energy Dispersive X-Ray
FFT	Fast Flux Test Facility
HLW	High Level Waste
M&O	Management and Operating Contractor
MDR	Material Degradation and Release
QA	Quality Assurance
SCFT	Solid-Centered Flow-Through
SEM	Scanning Electron Microscope
TST	Transition State Theory
UZ	Unsaturated Zone
WP	Waste Package
XRD	X- Ray Diffraction

1. PURPOSE

The purpose of this Analysis and Modeling Report (AMR) is to validate the Material Degradation and Release (MDR) model that predicts degradation and release of radionuclides from a degrading waste package (WP) in the potential monitored geologic repository at Yucca Mountain. This AMR is prepared according to *Technical Work Plan for: Waste Package Design Description for LA* (Ref. 17).

The intended use of the MDR model is to estimate the long-term geochemical behavior of waste packages (WPs) containing U. S. Department of Energy (DOE) Spent Nuclear Fuel (SNF) codisposed with High Level Waste (HLW) glass, commercial SNF, and Immobilized Plutonium Ceramic (Pu-ceramic) codisposed with HLW glass. The model is intended to predict (1) the extent to which criticality control material, such as gadolinium (Gd), will remain in the WP after corrosion of the initial WP, (2) the extent to which fissile Pu and uranium (U) will be carried out of the degraded WP by infiltrating water, and (3) the chemical composition and amounts of minerals and other solids left in the WP. The results of the model are intended for use in criticality calculations.

The scope of the model validation report is to (1) describe the MDR model, and (2) compare the modeling results with experimental studies. A test case based on a degrading Pu-ceramic WP is provided to help explain the model.

This model does not directly feed the assessment of system performance. The output from this model is used by several other models, such as the configuration generator, criticality, and criticality consequence models, prior to the evaluation of system performance.

This document has been prepared according to AP-3.10Q, *Analyses and Models* (Ref. 2), and prepared in accordance with the technical work plan (Ref. 17).

2. QUALITY ASSURANCE

An activity evaluation (Ref. 17, Addendum A), which was prepared per AP-2.21Q *Quality Determinations and Planning for Scientific, Engineering, and Regulatory Compliance Activities* (Ref. 1), determined that the Quality Assurance (QA) program (Ref. 45) applies to the activity under which this analysis was developed.

With regard to the development of this document, the control of the electronic management of data was evaluated in accordance with AP-SV.1Q *Control of the Electronic Management of Information* (Ref. 5). The evaluation determined that current work processes and procedures are in accordance with the controls specified in the technical work plan (Ref. 17).

3. COMPUTER SOFTWARE AND MODEL USAGE

3.1 SOFTWARE

This section describes the computer software used in the model. The software was used in a Pu-ceramic test case (Ref. 15).

Table 3-1: Computer Software Used in the Model

Software Name	Version	Software Tracking Number (Qualification Status)	Description and Components Used	Input and Output Files ^a (Included in Attachment I)
EQ3/6	7.2b	Qualified LLNL:UCRL-MA-110662 EQ3/6, Ref. 27	EQ3NR: a speciation-solubility code	input: *.3i pickup: *.3p output: *.3o
			EQPT: a data file preprocessor	input: data0.* output: data1.*
EQ6	7.2bLV	Qualified 10075-7.2bLV-00 EQ6, Ref. 31	EQ6: a reaction path code which models water/rock interaction or fluid mixing in either a pure reaction progress mode or a time mode	input: *.6i pickup: *.6p output: *.6o *.elem_aqu.txt *.elem_min.txt *.elem_tot.txt *.min_info.txt .bin
ASPRIN	1.0	Qualified 10487-1.0-00 ASPRIN, Ref. 18	ASPRIN: performs post-processing of numerical information (from an output data file created by EQ6), to calculate isotopic inventories for elements of interest	input: *.bin (from EQ6) output: *.txt
MS EXCEL	Version 97 SR-2	Commercial off-the-shelf software: Exempt in accordance with AP-SI.1Q Ref. 4, Section 2.1.	Excel: used in this document for graphical representation and arithmetical manipulations	input: *.elem_*.txt output: *.xls
PP	NA	Ref. 67. Used solely for visual display or graphical representation: Exempt in accordance with AP-SI.1Q Ref. 4, Section 2.1.2.	PP: a plotting tool used for graphical representation	input: *.bin (from EQ6) output: *.wmf

^a Files are explained in more detail in Attachment II.

In running the MDR model, EQ6 is run in the solid-centered flow-through (SCFT) mode. In this mode, an incremental amount of "fresh" water enters the WP system in each time step, displacing an equivalent volume of water out of the system.

For the test case, the software products were run on a standard personal computer, BSC Management and Operating Contractor for the Department of Energy's Office of Civilian Radioactive Waste Management Las Vegas Office, CPU # 117728. All applicable products were obtained from Software Configuration Management (SCM). The software was appropriate for

the application and was used within the range of validation in accordance with AP-SI.1Q (Ref. 4). However, some runs simulated periods of high ionic strength (1 to ~4). While EQ6 is capable of handling high ionic strengths, there is no Yucca Mountain Project (YMP)-qualified thermodynamic database with corrections for high ionic strength. To address this issue, several sensitivity tests were performed. (See Assumption 5.6).

3.2 MODELS

The mathematical model *Defense High Level Waste Glass Degradation* was used for degradation rate expressions for dissolution of glass immersed in water for the Pu-Ceramic test case. Both the earlier version of the model (Ref. 33 and Equations 7 and 8) and the most recent version of the model (Ref. 39 Equations 7 and 8) were used. Even though newer degradation rates were available, the earlier version of the model was used because it provides more conservative results than the most recent version of the model with regards to external and internal criticality (Ref. 15, Section 6.8.2 and 6.8.4).

The HLW glass degradation model does not have a Model Warehouse Data Tracking Number. The use of the model is justified, since the purpose of the model is to describe the degradation of HLW glass in a flooded waste package. The equations were converted to units appropriate for input into EQ6 in 'HLW_glass REV01.xls', sheet 'rates' (Attachment I).

4. INPUTS

4.1 DATA AND PARAMETERS

Table 6-1 through Table 6-4 list the inputs used in the model for the Pu-ceramic test case. The inputs are appropriate for the model because they have been developed or measured specifically for use in modeling processes at the potential repository.

4.1.1 Densities and Molecular Weights of Solids

The qualified EQ6 database, 'data0.ymp' (Ref. 59), does not contain molar volumes for some of the solids that were predicted to form during the EQ6 runs. If molar volumes of any of the solids are missing from the EQ6 database, then EQ6 does not add the volumes of those solids when calculating the volume of solids formed. To get a more accurate value of the volume of solids from EQ6, the molar volumes of several minerals were added to the database. The resulting file is named 'data0.yme'. Molar volumes for the solids were calculated from the molecular weights of the solids in 'data0.ymp' and the solid densities from various sources, as noted in Table 4-1. The current version of EQ6 (Section 3.1) performs the volume calculations for the minerals formed automatically.

Table 4-1. Densities, Molecular Weights and Molar Volumes of Precipitated Solids

Solid	Molecular Weight (g/mole) ^c	Molar Volume (cm ³ /mole) ^g	Calculated Density (g/cm ³)
Anatase (TiO ₂)	79.866	20.450	3.905 ^a
Berlinite (AlPO ₄)	121.953	46.2	2.64 ^a
CaUO ₄	342.105	45.865	7.459 ^b
Cr-ettringite (Ca ₆ Al ₂ (CrO ₄) ₃ (OH) ₁₂ ·26H ₂ O)	1314.888	726.900	1.809 ^b
Cr-ferrihydrite (Fe ₄ (CrO ₄)(OH) ₁₀)	509.444	129.000	3.96 ^f
Cu ₃ (PO ₄) ₂	380.581	84.520	4.503 ^b
Fe ₂ (MoO ₄) ₃	508.173	131.850	3.85
Fluorapatite [Ca ₅ (PO ₄) ₃ F]	504.302	157.594	3.2 ^a
GdOHCO ₃	234.266	737	0.318 ^b
Hydroxylapatite [Ca ₅ (PO ₄) ₃ OH]	502.311	163.088	3.08 ^a
KNpO ₂ CO ₃	368.106	68.160	5.401 ^b
Mesolite (Na _{0.676} Ca _{0.657} Al _{1.99} Si _{3.01} O ₁₀ ·2.647H ₂ O)	387.783	171.661	2.259 ^a
Na ₄ UO ₂ (CO ₃) ₃	542.013	149.305	3.63 ^b
Ni ₃ (PO ₄) ₂	366.023	83.263	4.396 ^b
NpO ₂	268.999	24.220	11.11 ^d
PuO ₂	275.999	23.830	11.581 ^e
α-Uranophane [Ca(UO ₂ SiO ₃ OH) ₂ ·5H ₂ O]	856.392	223.601	3.83 ^a
(UO ₂) ₃ (PO ₄) ₂ ·6H ₂ O	1108.118	316.605	3.5 ^b
Zn ₂ SiO ₄ (Willemite)	222.863	55.200	4.04 ^a

Sources: ^a Ref. 62 pp. 26 (anatase), 83 (berlinite), 289 (fluorapatite), 389 (hydroxylapatite), 547 (mesolite), 903 (α-uranophane), and 946 (Zn₂SiO₄).

^b Ref. 52, JCPDS cards for Ni₃(PO₄)₂ (38-1473), (UO₂)₃(PO₄)₂·6H₂O (30-1405), CaUO₄ (44-583), Na₄UO₂(CO₃)₃ (11-81), Cr-ettringite (41-218), Cu₃(PO₄)₂ (70-494), GdOHCO₃ (24-421), KNpO₂CO₃ (17-264).

^c Attachment I (EQ3/6 Data base, 'data0.yme').

^d Ref. 73 (p. B101).

^e Ref. 46 (p.C-103).

^f Ref. 70 (p. 386).

NOTES: ^g Calculated from the molecular weight and density.

Values for Molecular Weights may differ from those cited in the references for Calculated Density, but the difference is less than 1% and is not expected to affect the results of this calculation.

4.1.2 Thermodynamic Database

The thermodynamic database used for the EQ6 calculations, ‘data0.yme’, is a slightly altered version of the qualified database: ‘data0.ymp.R0’ (Ref. 59), with the following changes:

- Several Cr- and Fe-bearing minerals and an aqueous species [Cr-ettringite ($\text{Ca}_6\text{Al}_2(\text{CrO}_4)_3(\text{OH})_{12}\cdot 26\text{H}_2\text{O}$), Cr-ferrihydrite ($\text{Fe}_4(\text{CrO}_4)(\text{OH})_{10}$), $\text{CaCrO}_4^{\text{aq}}$, and $\text{Fe}_2(\text{MoO}_4)_3$] were added for a more complete database. The logK values were calculated in Ref. 16 (p. 15). Although unqualified, the data for the minerals that were added to the database come from the peer-reviewed literature, and consequently, the impact of any errors likely to be produced is believed to be small.
- GdOHCO_3 solubility was added to the database. The logK was assumed to be the same as the logK for NdOHCO_3 in the ‘data0.ymp.R0’ since Gd and Nd are both lanthanides and chemically similar (Assumption 5.15).
- The logK of GdHPO_4^+ was found to be incorrect in the database and changed from the value of 185 to -5.7 to match the value given in Ref. 66 (p. 39), which is the source listed in the database for that reaction.
- Molar volumes of the minerals in Table 4-1 were added to the database in order to calculate the density of the degradation products that are formed during the calculations.
- The HLW glass (composition given in Table 6-2) and the GICI glass (composition given in Table 6-10) were added to the database in order to take advantage of EQ3/6’s ability to use a pH-dependent rate law, using the EQ6 transition state theory (TST) formalism to describe the degradation. Only reactants entered as “minerals” (solids contained in the database) can specify a range of degradation rates based on pH; “special reactants” (reactants not contained in the database) must have a fixed degradation rate.

4.2 CRITERIA

The model validation presented in this document followed the guidance of NUREG 1636, (Ref. 48).

4.3 CODES AND STANDARDS

None Used.

5. ASSUMPTIONS

- 5.1 It is assumed that the solutions that drip into the waste package will have the major ion composition of J-13 well water as given in Ref. 58, and that minor components in the solution can be approximated by Ref. 50 (Table 4.2) for $\sim 6 \cdot 10^5$ years. The rationale for this assumption is that the groundwater composition is controlled largely by transport through the host rock, over pathways of hundreds of meters, and the host rock composition is not expected to change substantially over 10^6 years. This assumption is justified by recent evaluations of codisposal waste packages (Ref. 25) which show that degradation of the waste package materials (specifically, HLW glass and steel) overwhelms the native chemistry of the incoming water. (Figures 5-2 through 5-20 of Ref. 25 show pH variations of 3 to 10 in the waste package.) This assumption is used in Section 6.2.1 (Step 8) and 6.2.2.
- 5.2 The assumption that the water entering the waste package can be approximated by the J-13 well water implicitly assumes that any effects of contact with the engineered materials in the drift will be minimal after a few thousand years. For a few thousand years after waste emplacement, the composition may differ because of perturbations resulting from reactions with engineered materials and from the thermal pulse. These are not taken into account in this calculation because the outer shell and inner liner are not expected to breach until after that perturbed period. Therefore, the early perturbation is not relevant to the calculations reported in this document. This assumption is used in Section 6.2.1 (Step 8).
- 5.3 It is assumed that an aqueous solution fills all voids within the waste package and circulates freely in the partially degraded waste package so that all degraded solid products will react with each other through the aqueous solution medium. The rationale for this assumption is that sufficient decay heat will be retained within the waste package over the time of interest to cause convective circulation and mixing of the water inside the waste package (Ref. 22, Att. VI). Additionally, this assumption provides the maximum aqueous degradation of waste package components (with the potential for precipitation of radionuclides within the waste package) or the flushing of radionuclides from the waste package, and is therefore conservative. This assumption is used in Section 6.1.
- 5.4 It is assumed that the density of the incoming water is 1.0 g/cm^3 . The rationale for this assumption is that for dilute solutions, the density is extremely close to that of pure water, and that any differences are insignificant in respect to other uncertainties in the data and calculations. Moreover, this value is used only initially in EQ3/6 to convert concentrations of dissolved substances from parts per million to molalities. This assumption is used in Section 6.2.1 (Step 8).
- 5.5 It is assumed that 25°C thermodynamic data can be used for the calculations. The rationale for this assumption is two-fold. First, though the initial breach of the WP may occur at 10,000 years, when the WP contents are at temperatures $\sim 50^\circ\text{C}$ (Ref. 36, Figure 4.6-2, p. F4-49), at times $> 25,000$ years, the WP temperatures are likely to be close to 25°C . Second, the assumption is conservative with respect to loss of the Gd, the internal criticality control material. Gd phosphates are likely to be the solubility-limiting solids for the Gd. Since the solubility of gadolinium phosphate decreases with increases in

temperature (Ref. 49, Tables IV and V), use of the lower-temperature database is likely to be conservative. Additionally, the solubilities of actinides decrease with temperature, which is likely to be conservative for internal criticality (Ref. 47). This assumption is used in Section 6.2.1 (Step 13).

5.6 It is assumed that the EQ3/6 results generated using the B-dot activity model for solutions with ionic strength greater than 1 molal (M) are sufficiently accurate for the current calculation. (It is accepted that the B-dot activity model is accurate for ionic strengths *less* than 1 M.) The rationale for this assumption is that experimental data (a sensitivity test comparing EQ3/6 results with experimental results in sulfate, nitrate, and chloride solutions) shows that EQ3/6 results using the B-dot activity model can be used qualitatively up to an ionic strength of about 4 M to indicate the general nature of the reactions that would actually occur (Ref. 24, Appendix D). Another sensitivity test compared EQ6 results against experimental results in a carbonate system containing uranium (Ref. 35, Section 5.1.2). The conclusion was that the B-dot activity model overestimated the concentration of U in solution by an order of magnitude or greater. This is conservative for external criticality because it maximizes the U loss from the waste package. It may also significantly overestimate the accumulation external to the waste package (Ref. 35, Section 5.1.2). For internal criticality calculations, it may also be conservative with respect to gadolinium loss, if the concentration of Gd in solution is calculated to be higher than it would be in reality, as is the case for uranium. For internal criticality calculations, with respect to uranium loss, it may not be conservative in all cases. However, the cases chosen for internal criticality calculations have 100% or close to 100% of the uranium retained in the waste package (because these cases have the greatest potential for criticality), so the concentration of U in solution is inconsequential. This assumption is used in Section 6.2.1 (Step 13) and Section 3.1.

5.7 In general, it is assumed that chromium and molybdenum will oxidize fully to chromate (or dichromate) and molybdate, respectively. This assumption is based on the available thermodynamic data (Ref. 59), which indicate that in the presence of air, the chromium and molybdenum would both oxidize to the VI valence state. Laboratory observation of the corrosion of Cr and Mo containing steels and alloys, however, indicates that any such oxidation would be extremely slow. In fact, oxidation to the VI state may not occur at a significant rate with respect to the time frame of interest, or there may exist stable Cr(III) solids that substantially lower aqueous Cr concentration. For the present analyses, the assumption is made that, over the times of concern, oxidation will occur. The rationale for this assumption is that by allowing the Cr and Mo to oxidize, the pH of the system will be lowered allowing for the removal of neutron absorbers. This is conservative for internal criticality since the solubility of $\text{GdPO}_4 \cdot 10\text{H}_2\text{O}$ (the expected solubility-controlling phase for Gd) increases at lower pH (Ref. 25, Section 5.3.1). The resulting transport of Gd out of the waste package will separate the neutron absorber preferentially from the fissile material. This assumption is used in Section 6.1.

5.8 It is assumed that gases in the WP solution remain in equilibrium with the ambient atmosphere outside the WP. In other words, contact of WP fluids with the gas phase in the repository is envisioned to be sufficient to maintain equilibrium with the CO_2 and O_2 present, whether or not this is the normal atmosphere in open air or rock gas that seeps out of the adjacent tuff. Moreover, the specific partial pressures of CO_2 and O_2 of the ambient repository atmosphere are set to, respectively, $10^{-3.0}$ and $10^{-0.7}$ bar. The rationale

for the oxygen partial pressure is that it is equivalent to that in the atmosphere (Ref. 74, p. F-210). The rationale for choosing the carbon dioxide pressure is to reflect the observation that J-13 well water appears to be in equilibrium with above-atmospheric carbon dioxide levels (Ref. 78, Table 7). However, it is recognized that local reducing conditions may exist within the WP. The consequences and likelihood of such conditions are discussed in Section 6.2.6, and this assumption is also used in Section 6.1 and Section 6.2.1 (Step 8).

- 5.9 It is assumed that precipitated solids are deposited in the WP, remain in place, and are not mechanically eroded or entrained as colloids in the advected water. The rationale for this assumption is that it conservatively maximizes the amount of potential deposits of fissile material inside the waste package. This assumption is used in Section 6.1.
- 5.10 It is assumed that the corrosion rates used in this calculation encompass rates for microbially assisted degradation, and that the degradation rates will not be controlled principally by bacteria (Ref. 43, p. 3-84). The rationale for this assumption is (1) steel corrosion rates measured under environmental conditions inherently include exposure to bacteria, and (2) the lack of organic nutrients available for bacterial corrosion will limit the involvement of bacteria. This assumption is used in Section 6.2.1 (Step 7).
- 5.11 It is assumed that the drip rate into the WP varies from 1.5 to 500 l/y. Two factors influence the WP water flux: the drift seepage rate and the number of openings in the DS/WP system. The low end of the range corresponds to a low drift seepage rate or to a higher drift seepage rate with diversion of the bulk of water. The high end of the range represents a high drift seepage rate with little WP/DS diversion. This assumption is used in Section 6.2.3.
- 5.12 It is assumed that the reported alkalinity in analyses of J-13 well water corresponds to bicarbonate (HCO_3^-) alkalinity. The assumption is justified by two factors. First, the concentrations of borate, phosphate and silicate (other contributors to alkalinity), in J-13 well water, are small compared to bicarbonate concentration. Second, in most calculations, the imposed fCO_2 will control the dissolved bicarbonate concentrations; that is, the initial bicarbonate concentrations will not be tied to assumptions about alkalinity. The same assumption is implicitly made in Ref. 58. This assumption is used in Section 6.2.1 (Step 8).
- 5.13 It is assumed that the high-level waste glass composition is as given in Ref. 28 (Attachment I, p. I-7), and that the density of the high level waste glass is 2.85 g/cm^3 (Ref. 12, p. 26, Fig. 2, and pp. 54-57). The rational for this assumption is that the references cited above are the most recent and comprehensive sources available to provide this information. Additionally, glass composition sensitivity studies show that large variations in glass composition had little effect on Gd loss (Ref. 29, Section 5.3.3). This assumption is used in 6.2.1, and Table 6-2.
- 5.14 It is assumed that freshly precipitated minerals dissolve and grow instantaneously to maintain equilibrium with adjacent fluids. The basis for this assumption is that over the long time periods considered in running the model ($>100,000$ years), the impact on the results is minimal. Where appropriate, a sensitivity study is performed to evaluate the effect of kinetically-limited precipitation (Section 6.3.1.3). This assumption is used in Section 6.1.

5.15 It was assumed that the logK value for GdOHCO_3 is the same as the logK for NdOHCO_3 in the 'data0.ymp.R0' and 'data0.yme' databases. The rationale for this assumption is that Gd and Nd are both lanthanides and chemically similar. Further justification for this assumption can be found in Ref. 29 (Section 5.3.1). This assumption was used in Section 4.1.2.

5.16 It is assumed that the thermodynamic behavior of hafnium (Hf) can be treated as if it were zirconium (Zr). The rationale for this assumption is the extreme similarity of the chemical behaviors of the two elements (Ref. 54 , p. 272). Thermodynamic data for many important Hf solids and aqueous species are lacking, thus Zr was substituted for Hf in the calculation. This assumption is used in Section 6.2.1.

6. MODEL

Based on the screening criteria provided in AP-3.15Q, *Managing Technical Product Inputs*, (Ref. 3) this AMR does not include estimates of any “Principal factors” or “Other Factors” and is thus assigned an importance level of 3 per AP-3.10Q (Ref. 2).

6.1 CONCEPTUAL MODEL

The conceptual model consists of aqueous solutions entering and exiting a breached WP at constant and equal rates. The aqueous solution fills all voids within the waste package (Assumption 5.3). Water circulates freely enough in the partially degraded waste package that all degraded solid products react with each other through the aqueous solution medium (Assumptions 5.3). WP component steels and fuels react with these solutions according to kinetic rate expressions, forming a variety of secondary oxide and clay phases in the process. Chromium and molybdenum oxidize fully to chromate (or dichromate) and molybdate, respectively (Assumption 5.7). Formation of secondary phases and speciation of the aqueous phase is assumed to be instantaneous (Assumption 5.14), as is equilibration with ambient carbon dioxide and oxygen (Assumption 5.8). Precipitated solids deposited in the WP, remain in place, and are not mechanically eroded or entrained as colloids in the advected water (Assumption 5.9).

6.2 MODEL IMPLEMENTATION

6.2.1 Step-By-Step Model Description

The step-by step description provides the names (in parenthesis) of example files (located in Attachment I) that demonstrate each step. The example files come from EQ6 calculations for Pu-ceramic waste packages (Ref. 15, Ref. 30, and Ref. 35).

Step 1—Calculate the volume and surface area of each component of the waste package. (example: folder ‘Pu 1999’, file ‘pu-ceramic.xls’, sheets ‘GPC & Outer Web’ and ‘Magazine, Can, Rack, Disk’ and folder ‘Pu 2001’, file ‘Sleeve.xls’)

Step 2—Calculate the void volume, where the void volume can also be thought of as the volume of water that would fill a flooded waste package. This is necessary because EQ6 calculations are based on 1 liter of solution. This is calculated by summing the volume of each component in the waste package and subtracting from the inside volume of the waste package shell. (example: folder ‘Pu 1999’, file ‘pu-ceramic.xls’, sheet ‘Void&Norm’)

Step 3—Calculate the moles of each component. EQ6 requires that the quantity of each component be expressed in moles, rather than mass. To do this, the molecular weight of the material must be defined. In the example, a mole of each component (except the aqueous displacer) is defined as 100 grams. Therefore, the mass of a component divided by 100 g/mole gives the moles of the component. (Example for combined Steps 3 and 4: folder ‘Pu 1999’, file ‘pu-ceram.xls’, sheet ‘Void&Norm’ and folder ‘Pu 2001’, file ‘Sleeve.xls’)

Step 4—Calculate the normalized moles and normalized surface area of each component by dividing the moles and surface area calculated in Steps 1 and 3 by the void volume calculated in Step 2. The normalized moles and surface area represent the moles and surface area that would

contact 1 liter of solution. The normalized values are entered into the EQ6 input file. (example for combined Steps 3 and 4: folder 'Pu 1999', file 'pu-ceram.xls', sheet 'Void&Norm' and folder 'Pu 2001', file 'Sleeve.xls')

Step 5—Determine surface area corrections, if any, based on expected cracking of material or based on cladding integrity. If the fuel or HLW glass is expected to be fractured, the surface area is increased. In the Pu-ceramic example, the HLW glass surface area is increased by a factor of 21 due to cracking, and the surface area of the Pu-ceramic is increased by a factor of 30 to account for radiation damage (Ref. 35, Section 5.3.1.2). For fuels with a robust cladding that may delay degradation, a factor less than 1 may be employed. In the case of Shippingport LWBR SNF (Ref. 34), the calculated surface area was reduced to 1% and 10% for sensitivity runs, to account for the corrosion-resistant Zircaloy cladding.

Step 6—Calculate the molar composition (based on 100 g/mole) of each material in all components and enter into the EQ6 input file. This step calculated the moles of each element in 100 grams of material. (example: folder 'Pu 1999', file 'pu-ceramic', sheet 'Compositions', rows 135-143)

Step 7—Determine a degradation rate or a range of degradation rates for each material in units of "moles/(cm²·s)" (Assumption 5.10). The best available sources are used. Tables 1 through 3 from Ref. 15 (Section 5.1.2) provide the values and the sources for the degradation rates and the compositions used for Pu-ceramic. The HLW glass degradation rate in Table 6-2 is not a constant value; it is pH-dependent. The file 'HLW Glass REV01.xls' in folder 'Pu 2001' shows how the degradation rate values for the EQ6 input file were calculated. The file also provides a plot of the degradation values used in the calculations. In order to use the pH-dependent rate, the composition of the HLW glass (Table 6-2) was entered into the database as a mineral called "GlassSRL". The database is provided in folder 'databases', file 'data0.yme'. The actual rate in which the material degrades is the product of the degradation rate (EQ6 variable: rk1) and the surface area (EQ6 variable: sk).

Step 8—Determine the composition of the aqueous solution entering the waste packages (Assumption 5.4). In the example case, the composition of J-13 well water was used (Assumption 5.1, 5.2, and 5.12). See Section 6.2.2 for further discussion on incoming water. The fugacity of CO₂ and O₂ are fixed at 10⁻³ and 10^{-0.7} bars in most cases (Assumption 5.8). For sensitivity tests, higher values of CO₂ are used (Ref. 29, Section 5.3.2), lower values of CO₂ are used (Ref. 29, Section 6.2), and cases where the value of O₂ and CO₂ are determined by in-package competition between diffusion and degradation (Ref. 35, Section 6.3).

Step 9—Determine range of drip rates for incoming water, normalize the rates based on 1 liter, and convert to units of "moles/s" for input into EQ6. In the example, the drip rates in Table 6-4 were used (Ref. 15, Table 5-7). See Section 6.2.3 for discussion on drip rate.

Step 10—Determine sequence of degradation. In the example, two types of sequences of degradation were used—a one stage, in which all of the components degraded simultaneously and a two stage, in which some of the components (Pu-ceramic and the stainless steel cans) were not introduced until the second stage. See Section 6.2.4 for discussion of sequence of degradation.

Step 11—Determine runs to perform, varying degradation rates, drip rates, and sequence of degradation. Table 6-6 and Table 6-7 provide the list of cases that were run for the example case (Ref. 15, Tables 5-8 and 5-9).

Step 12—Determine the minerals to suppress. See Section 6.2.5 for discussion of suppressed minerals.

Step 13—Choose a qualified thermodynamic database (Ref. 59). If changes are needed, document and justify changes (Assumption 5.5 and 5.6).

Step 14—Run EQ6 using a batch file that renames the outputs and indicates the options that are used. The following is an example batch file:

```
del elem0aqua.bin
del mwmax.txt
copy decay.eq6.24100 decay.eq6

runeq6 yme p51rLx41.6i
move hwsdata p51rLx41.bin
move min_info.txt p51rLx41.min_info.txt
move elem_aqua.txt p51rLx41.elem_aqua.txt
move elem_min.txt p51rLx41.elem_min.txt
move elem_tot.txt p51rLx41.elem_tot.txt

del decay.eq6
```

Step 15—Tabulate the losses of neutron absorbers (such as gadolinium, Gd) and actinides (Pu and U). Table 6-8 is an example table containing results from the Pu-ceramic cases (Ref. 15, Table 6-16)

Step 16—For internal criticality calculations, calculate the density and mass of the corrosion products as a function of time for the cases with most conservative results (high Gd loss and low actinide loss). The density and mass are calculated using the ‘*.elem_min.txt’ output file. Table 6-9 is an example for one of the Pu-ceramic cases with high Gd loss, Case s10 (Ref. 15, Table 6-27). (example: folder ‘Pu 2001’, file ‘density_pu-ceramic.xls’, sheet ‘density’.)

Step 17—For external criticality calculations, calculate the U enrichment fraction (molar ratio of U-235 to total U) of the aqueous solution using ASPRIN software for the cases with the most conservative results (high Pu discharged from the waste package or high Pu and U loss).

Figure 6-1 is a plot from Pu-ceramic for a case with high Pu discharged from the waste package, Case s5 (Ref. 15, Figure 6-25).

Table 6-1: Steel Compositions, Densities, and Degradation Rates

Element	A516 Carbon Steel		316L Stainless Steel		304L Stainless Steel	
	(wt%) ^a	(moles) ^b	(wt%) ^c	(moles) ^b	(wt%) ^d	(moles) ^b
C	0.28	2.3312E-02	0.030	2.4977E-03	0.03	2.4977E-03
Mn	1.045	1.9021E-02	2.000	3.6405E-02	2.00	3.6405E-02
P	0.035	1.1299E-03	0.045	1.4528E-03	0.045	1.4528E-03
S	0.035	1.0915E-03	0.030	9.3557E-04	0.03	9.3557E-04
Si	0.29	1.0326E-02	1.000	3.5606E-02	0.75	2.6704E-02
Cr	0	0	17.000	3.2695E-01	19.00	3.6541E-01
Ni	0	0	12.000	2.0446E-01	10.00	1.7039E-01
Mo	0	0	2.500	2.6058E-02	0	0
N	0	0	0.100	7.1394E-03	0.10	7.1394E-03
Fe	98.315	1.7604E+00	65.295	1.1692E+00	68.045	1.2184E+00
Total	100.00	1.8153	100.000	1.8107	100.00	1.8294
Density (g/cm³)	7.85^e		7.98^f		7.94^f	
Rate	(μm/y)	(moles/(cm ² ·s)) ^g	(μm/y)	(moles/(cm ² ·s))	(μm/y)	(moles/(cm ² ·s))
Very Low	Same as average	Same as average	0.01 ^h	2.53E-15	Same as low	Same as low
Low	Same as average	Same as average	0.1 ⁱ	2.53E-14	0.1 ⁱ	2.52E-14
Average	72 ^j	1.79E-11	2 ^k	5.06E-13	34 ^k	8.55E-12
High	Same as average	Same as average	33 ^m	8.34E-12	208 ^m	5.23E-11

Sources: ^a Ref. 10 (p. 321, Table 1)

^c Ref. 9 (p. 2, Table 1)

^d Ref. 8 (p. 3, Table 1)

^e Ref. 7 (p. 9)

^f Ref. 11 (p. 7, Table XI)

ⁱ Ref. 23 (pp. 11-13)

^j Ref. 57 (pp. 2.2-96 – 2.2-98) were used to derive the corrosion rate in spreadsheet 'A516_Rate.xls', sheet 'prob', (Attachment I)

^k Ref. 38 (Figure 3-15, 50 percentile value)

^m Ref. 38 (Figure 3-15, 95 percentile value)

NOTES: ^b The moles of each element are calculated by dividing the weight percent by the atomic weight of each element

^g The molecular weight of each material is assumed to be 100 grams. The degradation rates in units of μm/y are multiplied by the density, divided by 10⁴ μm/cm, divided by 100 g/mole, divided by 365.25 days/y, and divided by 86,400 s/day to convert to units of moles/(cm²·s).

^h The very low rate for 316L was assumed to be 10 times lower than the low rate.

Table 6-2. Simplified Glass Composition, Density, and Degradation Rates

Element	Moles ^a	Comment
O	2.7038	
U	0.0078	
Np	0	Merged with U (~0.1% of actinides, ceramic Np overwhelms)
Pu	0	Merged with U (Pu ~1% actinides, ceramic Pu overwhelms glass Pu).
Ba	0.0011	
Al	0.0863	
S	0.0040	
Ca	0.0162	
P	0.0005	
Cr	0	Merged with Al (overwhelmed by steel Cr; Cr ₂ O ₃ similar to Al ₂ O ₃)
Ni	0	Merged with Fe
Pb	0	Merged with Ba (both form insoluble CrO ₄ ²⁻ compounds in EQ6 runs)
Si	0.7765	
Ti	0	Merged with Si (overwhelmed by ceramic Ti; TiO ₂ similar to SiO ₂)
B	0.2912	
Li	0	Merged with Na
F	0.0017	
Cu	0	Merged with Fe
Fe	0.1722	
K	0.0752	
Mg	0.0333	
Mn	0	Merged with Fe
Na	0.5767	
Cl	0	Removed (overwhelmed by Cl in in-dripping water)
Density ^b (g/cm ³)	2.85	
Total Rate Degradation Rate = $k_1[H^+]$ ^{0.04} + $k_2[H^+]$ ^{0.6} (moles/cm ² ·s)		
Average ^d	$k_1=8.86E-19$ liters/cm ² ·s	$k_2=7.98E-13$ liters/cm ² ·s
Moderately High ^d	$k_1=7.06E-18$ liters/cm ² ·s	$k_2=3.59E-12$ liters/cm ² ·s
High ^d	$k_1=1.08E-17$ liters/cm ² ·s	$k_2=4.87E-12$ liters/cm ² ·s
New Average ^c	$k_1=8.86E-19$ liters/cm ² ·s	$k_2=1.12E-11$ liters/cm ² ·s

Notes: ^a Simplified composition based on Ref. 28 (Assumption 5.13) as calculated in spreadsheet 'HLW_glass REV01.xls', sheet 'composition' (Attachment I). This composition was added to the 'data0.ymp' for the pseudo-mineral GlassSRL. One mole = 100g HLW glass.
^b Based on HLW glass density in Ref. 68, p. 2.2.1.1-4 (Assumption 5.13)
^c Ref. 39 (Equations 7 and 8); Converted to inputs for EQ6 in 'HLW_glass REV01.xls', sheet 'rates'.
^d Ref. 33 (Equations 7 and 8); Converted to inputs for EQ6 in 'HLW_glass REV01.xls'; sheet 'rates'.

Table 6-3. Composition and Degradation Rates of Pu-ceramic

Oxide	Composition		
	(wt%) ^a	(moles metal) ^b	(moles oxygen) ^c
CaO	10.0	1.78E-01	1.78E-01
HfO ₂ ^d	10.6	5.04E-02	1.01E-01
UO ₂ ^g	23.7	8.78E-02	1.76E-01
PuO ₂	11.9	4.35E-02	8.70E-02
NpO ₂	0.0	3.91E-04	7.82E-04
Gd ₂ O ₃	7.9	4.36E-02	6.54E-02
TiO ₂	35.9	4.49E-01	8.99E-01
Total	100.0	8.53E-01	1.51E+00
Density (g/cm ³)	5.5 ^e		
Rate	(moles/(cm ² ·s)) ^f	Basis	
Average	8.0E-16	Picked as factor of 10 lower than high value	
High	8.0E-15	Ref. 35, p. 27, based on 50°C rates for radiation-damaged ceramic from Ref. 63	
Very High	8.0E-14	picked as factor of 10 higher than high value	

Sources: ^a Ref. 56 (Table 3.1)

^e Ref. 64 (p. 3-4)

Notes: ^b Moles of metal is the weight percent oxide divided by the molecular weight of the oxide.

^c Moles of oxygen is the moles metal (calculated in the previous column) times the ratio of (moles oxygen)/(moles metal) in the formula for the oxide.

^d Replaced by Zr in EQ6 runs, then converted back to Hf for mass calculations.

^f One mole special reactant = 100 g.

^g The uranium is 1.69 wt% U-235, with the remainder U-238 (Ref. 64)

Table 6-4. Drip Rate Values for Input to EQ6

Drip Rate (m ³ /year)	Drip Rate (normalized for EQ6 input) (moles/s) ^a
0.0015	1.03E-11
0.015	1.03E-10
0.15	1.03E-09
0.5	3.45E-09

NOTE: ^a The values of drip rate in units of m³/year are multiplied by 1000 liters/m³, divided by 1 liter/mole, divided by 365.25 days/year, divided by 86,400 s/day, and divided by 4594 liters of void volume.

Table 6-5. EQ6 Input File Elemental Molal Composition for J-13 Well Water

Chemical Composition					
O	5.55E+01	Gd	1.00E-16	Na	1.99E-03
Al	1.00E-16	H	1.11E+02	Ni	1.00E-16
B	1.00E-16	C	2.07E-03	Np	1.00E-16
Ba	1.00E-16	P	1.00E-16	Pu	1.00E-16
Ca	3.24E-04	K	1.29E-04	S	1.92E-04
Cl	2.01E-04	Mg	8.27E-05	Si	1.02E-03
Cr	1.00E-16	Mn	1.00E-16	U	1.00E-16
F	1.15E-04	Mo	1.00E-16		
Fe	1.00E-16	N	1.42E-04		

Sources: from Ref. 40 (Table 6), based on Ref. 58. These values are outputs from EQ3NR for input into EQ6 input file.

Table 6-6. Summary of Single-Stage EQ6 Cases for Pu-Ceramic Waste Package

Case Number	Rates of Degradation ^a for:			Water Drip Rates (m ³ /y)	Comments ^b	Case ID
	Steel	Glass	Pu-ceramic			
3	Average	Average	High	0.0015	5 Pu canisters	p10_1131
5	Average	Average	Average	0.015	5 Pu canisters	p10_1122
8	Average	High	High	0.0015	5 Pu canisters	p10_1231
10	Average	High	Average	0.015	5 Pu canisters	p10_1222
14	High	Average	High	0.15	5 Pu canisters	p10_2133
s1	Average	Average	High	0.0015	1 Pu canister	p51_1131
s2	Average	Average	High	0.015	1 Pu canister	p51_1132
s3	Average	Average	High	0.0015	2 Pu canisters	p52_1131
s4	Low	High	Very High	0.0015	2 Pu canisters	p52rL241/p52sL241
s4b	Low	High	Very High	0.0015	2 Pu canisters	p53rL241/p53sL241
s5	Very Low	Moderately High	Very High	0.0015	2 Pu canisters	p52rLx41
s6	Average	Average	High	0.0015	5 Pu canisters, GdPO ₄ ·H ₂ O is formed	p60_1131
s9	Low	Average	High	0.015	2 Pu canisters	p52_L132
s10	Low	Average	Very High	0.015	2 Pu canisters	p52_L142
s11	Low	Average	High	0.15	2 Pu canisters	p52_L133
s12	Low	Average	Very High	0.15	2 Pu canisters	p52_L143
s13	Average	Average	High	0.015	2 Pu canisters	p52_1132
s14	Average	Average	Very High	0.015	2 Pu canisters	p52_1142
s15	Average	Average	High	0.15	2 Pu canisters	p52_1133
s16	Average	Average	Very High	0.15	2 Pu canisters	p52_1143
s17	Low	New Average	Very High	0.015	2 Pu canisters	p52_Ln42
s18	Average	New Average	Very High	0.15	2 Pu canisters	p52_1n43
s19	Low	New Average	Very High	0.0015	2 Pu canisters	p53rLn41
s20	Very Low	New Average	Very High	0.0015	2 Pu canisters	p52rLn41
s21	Very Low	Moderately High	Very High	0.0015	1 Pu canister	p51rLx41

NOTE: ^a See Table 6-1, Table 6-2, and Table 6-3 for numerical values of rates.

^b In the single-stage runs, hematite was the iron oxide allowed to form.

Table 6-7. Summary of Multiple-Stage EQ6 Cases for Pu-Ceramic Waste Package

Case Number	Rates of Degradation ^a for:			Water Drip Rates (m ³ /y)	Comments	Case ID	Fe Oxide
	Steel	Glass	Pu-ceramic				
21(a)	High	High	No Ceramic	0.5	5 Pu canisters	p11h2204	Hematite
21(b)	High	No Glass Present	Average	0.015	5 Pu canisters	p12h2022	Hematite
22(a)	High	High	No ceramic	0.5	5 Pu canisters	p11g2204	Goethite
22(b)	High	No Glass Present	Average	0.015	5 Pu canisters	p12g2022	Goethite
s7(a)	High	High	No ceramic	0.5	1 Pu canister	p71g2204/p72g2204	Goethite
s7(b)	High	No Glass Present	Average	0.015	1 Pu canister	p73g2022	Goethite
s8(a)	High	High	No ceramic	0.5	2 Pu canisters	p81g2204	Goethite
s8(b)	High	No Glass Present	Average	0.015	2 Pu canisters	p82g2022	Goethite

NOTE: ^a See Table 6-1, Table 6-2, and Table 6-3 for numerical values of rates.

Table 6-8. Result of Sensitivity Analyses

Sensitivity	Case ID	Root Name	Number of Pu Canisters	Years	%Gd Loss ^a	Initial Moles Pu	Moles Pu Discharged ^b	%Pu & U Loss ^a
Pu-Ceramic Loading	s1	p51_1131	1	6.34E+05	0.05	112	14.12	100.00
	s2	p51_1132	1	3.97E+05	0.21	112	12.24	100.00
	s3	p52_1131	2	6.34E+05	0.27	224	27.21	100.00
	s7	p71g2204/p72g2204/73g2022	1	4.36E+05	0.15	112	0.67	8.98
	s8	p81g2204/p82g2022	2	6.34E+05	0.25	224	0.79	6.10
Source Term	s4	p52rL241/p52sL241	2	6.34E+05	33.49	224	115.92	69.63
	s4b	p53rL241/p53sL241	2	6.34E+05	33.47	224	109.15	68.95
	s5	p52rLx41	2	6.34E+05	0.26	224	155.14	100.00
	s19	p53rLn41	2	6.34E+05	31.97	224	0.14	0.44
	s20	p52rLn41	2	6.34E+05	10.68	224	22.44	100.00
	s21	p51rLx41	1	6.34E+05	0.14	112	80.30	100.00
GdPO ₄ Hydration	s6	p60_1131	5	6.34E+05	0.24	558	51.82	100.00
Gd Loss	s9	p52_L132	2	2.19E+05	45.44	224	1.69	1.87
	s10	p52_L142	2	2.22E+04	77.92	224	0.81	0.22
	s11	p52_L133	2	9.69E+04	4.87	224	3.70	5.69
	s12	p52_L143	2	4.93E+04	23.48	224	3.19	2.79
	s13	p52_1132	2	1.55E+05	0.31	224	15.53	85.83
	s14	p52_1142	2	1.54E+04	41.95	224	3.80	0.58
	s15	p52_1133	2	1.04E+05	0.28	224	8.24	8.46
	s16	p52_1143	2	1.52E+04	58.61	224	4.12	1.83
	s17	p52_Ln42	2	5.19E+04	57.20	224	0.40	0.46
	s18	p52_1n43	2	1.53E+04	53.16	224	3.79	1.35

NOTE: ^a Calculated in file 'Summary Results.xls', sheet 'Total Elem' in Attachment II of Ref. 15 for Cases s1-s8.
 Calculated in 'calculate loss.xls' for Cases s9-s21.

^b Calculated in files 'p52{rs}L241 extended.xls', 'p53rL241 extended.xls', 'p52rLx41 extended.xls', 'p52rLn41.xls', and 'Pu_discharged_elem_aqu.xls' in Attachment II of Ref. 15.

Table 6-9. Composition of Corrosion Products^b (grams) and Density in Selected Years for Case s10 (p52_L142)

Element	Year				
	157	15154	22226	49918	630370
O	3.60E+02	4.87E+02	5.22E+02	6.58E+02	1.79E+03
Al	6.22E-02	5.54E-01	7.82E-01	1.67E+00	2.38E+01
B	0.00E+00	0.00E+00	0.00E+00	4.15E-14	0.00E+00
Ba	4.03E-03	3.29E-02	4.60E-02	9.71E-02	1.38E+00
Ca	3.31E-02	1.21E+00	1.13E+00	1.53E+00	1.54E+01
Cl	0.00E+00	1.90E-13	0.00E+00	0.00E+00	0.00E+00
Cr	0.00E+00	1.25E-02	1.74E-02	3.68E-02	0.00E+00
F	3.06E-03	2.22E-11	2.57E-19	0.00E+00	1.95E-01
Fe	8.16E+02	9.99E+02	1.07E+03	1.33E+03	2.89E+03
Gd	7.95E-02	3.82E+00	1.69E+00	1.69E+00	1.69E+00
H	3.15E-02	8.03E-01	8.90E-01	1.16E+00	6.60E+00
C	5.13E-13	2.71E-01	3.90E-13	0.00E+00	1.21E-01
P	5.58E-02	2.86E-01	3.33E-01	5.14E-01	1.56E+00
K	0.00E+00	2.54E-13	0.00E+00	0.00E+00	1.85E+00
Mg	0.00E+00	1.31E-12	2.97E-02	1.72E-01	5.74E+00
Mn	8.71E+00	1.41E+01	1.61E+01	2.37E+01	6.87E+01
Mo	1.16E-03	1.40E+00	1.44E+00	1.35E+00	9.61E-02
N	0.00E+00	1.45E-12	3.04E-18	0.00E+00	0.00E+00
Na	0.00E+00	8.53E-13	3.99E-17	0.00E+00	9.42E+00
Ni	0.00E+00	1.15E+01	1.31E+01	1.47E+01	1.85E+02
Np	0.00E+00	5.66E-02	3.33E-02	0.00E+00	0.00E+00
Pu	7.33E-02	7.46E+00	6.08E+00	2.73E+00	0.00E+00
S	9.38E-04	5.58E-11	0.00E+00	0.00E+00	0.00E+00
Si	3.04E+00	1.10E+01	1.44E+01	2.80E+01	3.01E+02
Ti	2.50E-01	2.41E+01	2.41E+01	2.41E+01	2.41E+01
U	2.84E-01	2.72E+01	2.87E+01	3.25E+01	4.87E+01
Hf(Zr) ^a	5.33E-02	5.13E+00	5.13E+00	5.13E+00	5.13E+00
Total (kg)	5459	7330	7827	9757	24727
Density (g/cm³)	5.27	5.21	5.16	5.10	4.59
%Gd loss	0.0	49.4	77.9	77.9	77.9
%U + PU loss	0.03	0.2	0.2	0.5	6
%Pu-ceramic left	99.0	0.0	0.0	0.0	0.0
%Glass left	99.8	98.6	98.1	95.9	41.9
%316NG WP Liner left	100.0	97.5	96.3	91.7	0.0

NOTES: ^a Hf was converted to Zr for EQ6, then converted back to Hf for mass and density calculations (See Assumption 5.16).

^b Mass of each element is based on 1 liter aqueous fluid. To obtain total grams of each element in waste package, multiply by total system volume of 4594 liters.

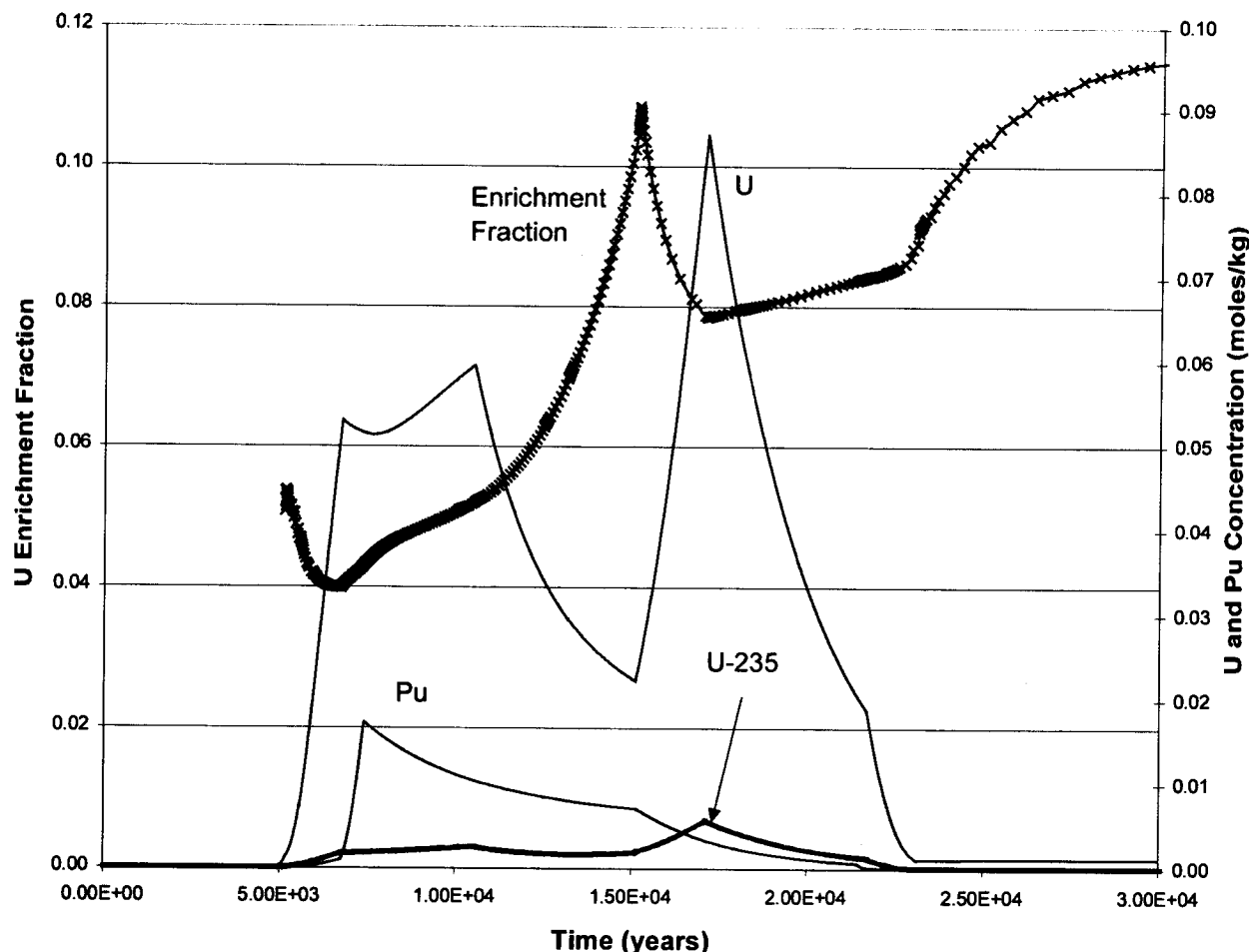


Figure 6-1: Case s5: Uranium Enrichment Fraction and Total Aqueous U and Pu

6.2.2 Incoming Water Composition

The water composition likely to enter the waste package cannot be predicted accurately ahead of time, but it most likely will be similar to some combination of the water found in the unsaturated zone today and saturated zone J-13 well water (Ref. 58). For the current application, we assume the chemical composition of the incoming water will have the major ion composition of J-13 well water (Assumption 5.1). Recent evaluations of codisposal waste packages (Ref. 14, Figures 7 and 8) and Pu-ceramic waste packages (Ref. 29, Figures 6-17 and 6-19) show that degradation of the waste package materials overwhelms the native chemistry of the incoming water, causing wide pH variations. A recent document (Ref. 16, Section 4.1.2) studied the impact of using alternate compositions for incoming water (evaporated J-13 water and simulated pore water). For degrading waste packages containing Fast Flux Test Facility (FFTF), Ref. 25, SNF or commercial SNF (CSNF), the pH profiles varied only slightly with the composition of the incoming water. The sensitivity of the incoming water composition to the output pH was insignificant compared to the effects of changing the drip rate or surface area of the fuel (Ref. 16, Section 6.2).

6.2.3 Drip Rate of Incoming Water

It is assumed (Assumption 5.11) that the drip rate onto a waste package is the same as the rate at which water flows through the waste package. (This rate is called the mean seep flow rate). The drip rates selected for this report correspond to reasonable percolation flux values as shown in Figure 3.2-15 of Ref. 36. A range of drip rates was chosen. Specifically, values of 0.0015, 0.015, and 0.15 m³/year were used for most cases, corresponding to percolation fluxes ranging from about 10 mm/year to 80 mm/year. The value of 10 mm/year corresponds to a high infiltration rate for the present-day climate and 80 mm/year corresponds to about twice the high infiltration rate for the glacial-transition climate (Ref. 36, Table 3.2-2). [Table 3.2-2 of Ref. 36 gives values of net infiltration rate, rather than percolation flux; however, they are equal at the potential repository level (Ref. 36, Section 3.2.3.4, p. 3-33)]. For a few runs, the range of allowed drip rates included an upper value of 0.5 m³/yr, which represents about 100 mm/year percolation flux.

6.2.4 Sequence of Degradation Scenarios

The rationale for selecting a particular scenario for degradation sequence for the EQ6 simulations is to provide conservative assessments of solubility and transport of criticality control materials (Gd and Hf, the neutron absorbers) and fissile materials (i.e., U and Pu compounds) in the waste package. For internal criticality, conservative conditions are those that maximize the loss of Gd from the waste package, while maintaining a high level of U and Pu within the waste package. For external criticality, conservative conditions must maximize the loss of Pu and U and minimizes the loss of neutron absorbers from the waste package and maintain a high aqueous concentration of U and Pu. It is important to maintain a high aqueous concentration of U and Pu to allow precipitation in the fractures and lithophysae beneath the degrading waste package. For external criticality, a high uranium enrichment (molar ratio of U-235 to total U) of the aqueous phase is also considered conservative.

The degradation scenarios are divided into two general categories. The first category comprises single-stage cases, in which all reactants (steels, HLW glass, and fissile materials) are exposed simultaneously to the water in the waste package. Because the reaction rates of the materials in the waste package may vary greatly, the materials do not necessarily coexist for the entire span of the EQ6 calculation. For example, the carbon steel support structure may be completely corroded within the first few hundred years, whereas stainless steel components, and the more durable fuel types, may remain, largely uncorroded, for $\sim 10^4$ to 10^5 years. The second category comprises two types of two-stage runs, referred to as Scenario I and Scenario II. For an example of a Scenario I two-stage run, consider the case of a Pu-ceramic waste package. The first stage involves exposing the A516 outer web (basket) and the GPCs (HLW glass and 304L steel) to water first, until the HLW glass is completely degraded and its alkalinity largely flushed out of the system. In the second stage, the 304L cans, magazines, rack, and Pu-ceramic disks are added as reactants. The aim of this two-stage run is to force a “conservative” condition of high acidity, by degrading the HLW glass rapidly, before all the acid-producing steel is degraded. For an example of a Scenario II two-stage run, consider the case of a Melt and Dilute codisposal waste package (Ref. 14, Section 5.2.2). The first stage involves an early breach of the 316L DOE canister containing the Melt and Dilute ingots, with everything degrading except the HLW glass. When the ingots degrade in this low pH environment, the uranium minerals are favored to form over the Gd minerals, and the Gd released from the ingots is flushed out of the package. In the second stage, the 304L canisters holding the HLW glass are allowed to breach.

6.2.5 Suppressed Minerals

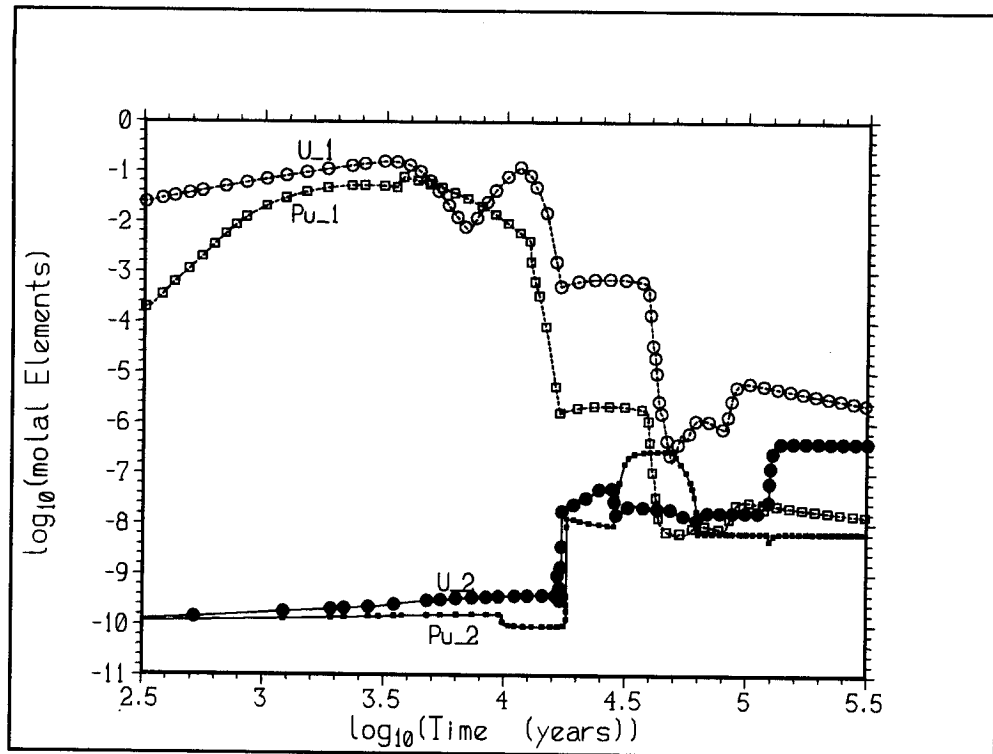
The following minerals were suppressed (not allowed to form) in many of the EQ6 runs: quartz, tridymite, muscovite, celadonite, dolomite, dolomite-dis, dolomite-ord, annite, and phlogopite. The dolomites, micas (muscovite, annite, and phlogopite), and celadonite were suppressed because they are extremely unlikely to form at low temperatures. The more stable quartz and tridymite were suppressed because the J-13 water is supersaturated with them (Ref. 16, p. 12). In some cases, the log K value of minerals are adjusted for sensitivity studies ($\text{Pu}(\text{OH})_4$ in Ref. 35, Section 5.1.3; CaUO_4 in Ref. 14, Section 6.2.3). In addition, in some cases the more stable iron and aluminum minerals are suppressed, such as hematite and diasporite, such that less stable goethite and gibbsite are formed.

6.2.6 Consequences of Lowered fO_2

Several sensitivity studies have shown that lowered fO_2 can dramatically reduce the loss of either actinides or Gd. For example, section 2 in Ref. 29 assessed the effect of simply lowering the fO_2 to 10^{-10} bars, from the default of $10^{-0.7}$ (0.2) bars. As shown in that calculation, 10^{-10} bars is not that “low” and is easily achievable in a natural, near-surface environment. The lowered fO_2 dropped calculated Gd loss from 20.45 to 1.3%, for a Pu-ceramic package, but had no significant effect on the Pu or U loss. Since the retention of Gd decreased the chance of internal criticality, use of atmospheric fO_2 (0.2 bars) was conservative. The cause of the reduced Gd loss was indirect. The lower fO_2 reduced acidity of the aqueous phase in the WP, by reducing the rate of acid production via oxidation of Cr (in steel) to CrO_4^{2-} . Since GdOHCO_3 is the major Gd-containing solid phase in the simulations, reduction of acidity decreased the loss of Gd from the WP.

A more mechanistic analysis of fO_2 variation was used in Ref. 35. It was recognized that some of the most aggressive chemical environments, as modeled by EQ6, occurred when either steel or glass degraded very rapidly. However, under such conditions, the buildup of corrosion products should also be fast, and should provide a diffusive barrier to oxygen. Since the corrosion of steel or reduced actinides consumes oxygen, it is easy to achieve a state where the competition between corrosion and diffusion limits the local fO_2 .

Figure 6-2, reprinted from Section 6.3 of Ref. 35, compares the aqueous U and Pu concentrations for a run in which the fO_2 is fixed at 0.2 bars (case 1), versus a run in which a diffusive boundary layer is allowed to limit oxygen ingress (case 2). For the latter case, a very modest boundary layer thickness of 1 cm was assumed. This boundary thickness is considered to be very conservative, since the calculation predicts corrosion products amounting to ~20% of the entire package void space within $\sim 2.10^3$ years. (20% corresponds to particle volume; the actual sedimented volume of clay-like material, including porosity, could be much higher). When the oxygen ingress is limited by diffusion through the boundary layer, the aqueous Pu and U concentrations are 6 to 9 orders of magnitude lower in the early part of the calculation. The concentrations rise only after the supply of reducing materials (steels and reduced actinides) is consumed. Thus for the initial $\sim 3.10^4$ years, the case 2 conditions generate a much lower “source term” for external criticality calculations.



(U_1 and Pu_1) model with fixed system $fO_2=0.2$

(U_2 and Pu_2) model with fO_2 determined by competition between diffusion (through a 1-cm boundary layer) and corrosion.

Figure 6-2: Aqueous U and Pu concentrations in the WP

6.3 MODEL VALIDATION

The MDR model is a combination of simpler sub-models for the corrosion behavior of DHLW glass, actinide ceramics (such as spent fuel), and steels. The corrosion sub-models depend, in turn, on accurate thermodynamic data to describe the stabilities of the corrosion products, and on reasonable kinetic data for the corrosion mechanisms. Confidence in the MDR model can be increased, if the corrosion sub-models of the individual components can be validated. Validation consists of showing that the methodology used in the MDR sub-models, when applied to controlled experiments or well-studied analogues, correctly predicts the sequence of corrosion products, or the concentrations of solutes in the coexisting aqueous phases.

In this section, the EQ6 simulations for glass and fuel degradation are validated. The focus on glass and fuel modeling is in response to the findings of the DOE-NRC technical exchange (Ref. 60). Specifically, subissues 3 and 4 addressed the need to validate fuel and glass corrosion models.

The corrosion chemistry of steels, under oxidizing conditions, is well studied, and is not discussed further in this document. Steel corrosion shows little dependence on $f\text{CO}_2$, at least for near-atmospheric levels (Ref. 6, p. 536). In the pH range of 4 to 10, the corrosion rate of iron depends little on pH, but the rate has a significant dependence on oxygen availability (Ref. 6, p. 515). Thus the validation of steel corrosion models, under varying $f\text{O}_2$, will be covered in upcoming calculations and analyses that focus on WP degradation under varied $f\text{O}_2$ conditions.

6.3.1 Glass Degradation Sub-Model

Studies of archeological stained glass (Ref. 20 and Ref. 19) were chosen to validate the glass corrosion sub-model. In these studies, Cooper and Cox estimated glass degradation rates from both MCC-4 lab experiments (Ref. 69) and examination of 450 year-old glass exhumed from soils near the River Ouse, in York, England (Ref. 53). Several aspects of the archeological glass studies make them suitable for validation, such as:

- (1) Some MCC-4 experiments were of sufficiently low temperature (85.5 °C) and sufficiently simple composition, to allow modeling via EQ6 at the same temperature. The glass had low corrosion resistance, and high alkali and alkaline-earth content, and is therefore more similar to waste glass than are natural analogues involving rhyolitic or basaltic glasses.
- (2) The tests did not reach saturation with amorphous silica, and therefore were unaffected by the $(1 - (Q/K))$ affinity term (where Q is the ion activity product, and K is an effective equilibrium constant (Ref. 39). Many glass dissolution tests are performed such that the affinity term is significant; however, the EQ6 simulations do not include an affinity term, so those tests are difficult to model.
- (3) The MCC-4 tests involve a flushed reactor, directly analogous to the SCFT model used in the MDR model. Ref. 20 reported that the initial agreement between the experiments and EQ6 was “not very encouraging;” however, they did not use a version of EQ6 with the SCFT capability, and did not attempt to include a pH dependence in the model.
- (4) The 450 year-old glass had significant corrosion crusts, and was likely in a state of constant dampness and constant contact with clay minerals, during its burial period. These conditions are reasonably analogous to those predicted for the MDR model. Measured pH (7.6, from Ref. 20) approximates values measured in wells from the proposed repository (Ref. 58).

- (5) The compositions and mineralogy of alteration products in both MCC-4 tests, and the buried archeological samples, are well documented; in most glass laboratory studies, the crusts are too thin, or too amorphous, for characterization.
- (6) The 450 year-old samples appear to have degraded faster than expected, based on MCC-4 and static Dickson autoclave experiments, suggesting a mechanism that must be explained to justify conservatism and the use of experimental results. The authors suggested a pH mechanism for increasing degradation rates, which is testable with EQ6.
- (7) The longevity of glass in the presence of clays has been questioned by Vernaz and Godon (Ref. 72, p. 30). This issue is relevant to the WP models, in which glass is expected to coexist with massive quantities of Fe-rich Si-poor nontronite clays. The Ouse region soils consist of clays, silts and limestone fragments (Ref. 53), and the interaction with clay was suggested as a cause of high corrosion rates by Ref. 20.

One disadvantage of the Cooper and Cox study is the lack of pH monitoring in the MCC-4 tests. However, simple mass-balance strongly constrains the pH of the solutions; and the pH is determined principally by the Na and K contents and the input rate for the MCC-4 tests. As will be shown, a variety of calculations converges on the same predicted pH.

6.3.1.1 Metrics for Validation

The first and most important metric is a comparison of model predictions with the types and amounts of minerals formed in the MCC-4 tests at 85.5 °C, and on the 450 year-old archeological samples. For the second metric, the EQ6 simulations should predict the anomalous, high degradation rates claimed for the buried glasses. Because of the uncertainties in the natural degradation environment, the prediction is really a defensible explanation of the causes for rate variations. The third metric is the prediction of Mg concentrations in the MCC-4 tests. This test is subject to substantial uncertainties, so the principal aim of the model is to show that with reasonable assumptions, the approximate Mg concentration will be estimated, within the uncertainty of rate and surface area estimates. The prediction of Na, K, Ca and Si aqueous concentrations is not a strong test, as these elements are not strongly controlled by alteration minerals, and the prediction would involve little more than a consistency check on rates reported in the journal article. Furthermore, Cooper and Cox (Ref. 20) provide Mg and Ca concentrations, but do not provide explicit measurements of aqueous Na, K and Si for the 85.5 °C tests.

The purpose of the glass models, as used for in-package criticality, is to provide reasonable constraints on the effects of glass degradation on in-package chemistry. In particular, the models bound the types and mass of degradation minerals and the alkalinity and pH of the aqueous solutions that coexist with degrading glass. The literature abounds with detailed models for prediction of glass behavior (Ref. 39); we do not attempt to validate such detailed models, but rather to validate the bulk chemical evolution of the glass-water system. The minerals predicted by EQ6 runs are taken to represent the alteration crusts that form in experiments and in analogues; however, the EQ6 simulations do not consider explicitly the physical location of the crusts.

The EQ6 simulations do not consider an affinity effect for three reasons:

- (1) it is generally conservative to ignore the affinity effect, and analyses have determined that the effect is unreliable as a means to slow glass degradation (Ref. 39)

- (2) studies show that the affinity effect may be ephemeral, because clay nucleation may cause a return to high rates and low solution silica contents (Ref. 72)
- (3) EQ6 does not provide a means to control the affinity term with an arbitrarily-selected set of aqueous species (e.g., SiO_2). In EQ6, the affinity term must use the full equilibrium constant K for the solid, and this constant is particularly meaningless for controlling glass degradation.

6.3.1.2 Methods: MCC-4 Models

Test 4a was selected (Table 2 in Ref. 20) because of its low temperature and comparatively long reaction time (i.e., long relative to the other low-T experiments). The temperature of this test (85.5 °C) is below the 100 °C limit of the current qualified thermodynamic database (Ref. 59). The MCC-4 tests involved continuous flow through a heated reactor vessel, and were modeled with the SCFT capability of EQ6 (Ref. 31). The authors specified that the test was run with deionized, distilled water; EQ3NR was used to provide an initial water composition (file stain00.3i), containing trace Na, K, Mg, Ca, P, and Si, and equilibrated to atmospheric CO_2 ($10^{-3.5}$ bar, Ref. 74, p. F-210) at 85.5 °C. This initial water was added to the model system as a “displacer” reactant, pushing an equal volume out of the vessel with each timestep. The vessel volume was taken as 80 cm^3 (Ref. 19, p. 527), the glass density as 2.62 g/cm^3 , the surface area as 4.5 cm^2 , and the water addition rate as 0.08 $\text{cm}^3/\text{minute}$ (Ref. 20). These physical quantities were scaled to a standard EQ6 system with an aqueous volume of 1000 cm^3 , via spreadsheet ‘glass_archeol.xls’ (folder ‘glass’, Attachment I).

The GICI glass composition from Table 1 of Ref. 20 was normalized to a molecular weight of 100 g in spreadsheet ‘glass_archeol.xls’, and presented in Table 6-10. A pseudo-mineral, GlassGICI, was created from this composition, and placed in the EQ6 database ‘data0.yme’ (Section 4.1.2). The glassGICI mineral was given a $\log_{10}K = 50$ for dissolution, which assures that the solid phase will never be stable under WP conditions. The pseudo-mineral was created purely to allow assignment of a TST rate law to the glass under EQ6.

Table 6-10: Simplified GICI Glass Composition

Element	Moles
O	2.5798
Na	0.0974
Mg	0.1845
Al	0.0315
Si	0.7711
P	0.0991
K	0.2966
Ca	0.3369
Mn	0.0241

Table 1 of Ref. 20, as simplified in ‘glass_archeol.xls’ (Attachment I)

Three types of EQ6 simulations, of increasing complexity, were used to simulate the MCC-4 test.

The first (Model A) employed a fixed glass dissolution rate, independent of pH, and equal to the normalized Na release rate given in Table 6 of Ref. 20; the conversion to EQ6 units is performed in spreadsheet 'glass_archeol.xls'. The input file used for this model is 'stain00A.6i'. However, it is apparent that the dissolution of the glass must have a dramatic effect on the system pH (Figure 6-5).

The second (Model B) used a pH-dependent glass dissolution rate, based on the functional form given by Ref. 39 (Section 6.1.1, equations 1 and 2, and Section 6.2.1.1) for the pH coefficients.

$$\text{Rate at low pH} = S.k_1 \cdot 10^{-0.6 \cdot \text{pH}} \cdot \exp(-E_a/RT)$$

Equation 1

$$\text{Rate at high pH} = S.k_2 \cdot 10^{0.4 \cdot \text{pH}} \cdot \exp(-E_a/RT)$$

Equation 2

where S is the surface area and the rate is given in mols/(cm².s), E_a is the activation energy in J/mole, and R is the gas constant in J/(mole.K). The k₁ and k₂ were obtained by successively incrementing the Ref. 39 values until the final, total dissolution rate matched the steady-state rate reported by Ref. 20. The files used for the incremental testing are named 'staine?a.6i', where ? is a number from 1 to 6 ('staine6a.6i' was the file that matched the observed steady-state glass rates).

Both Models A and B allow instantaneous precipitation of minerals (corrosion products) that achieve saturation. It is expected that these models will produce a rapid and unrealistic drop in the aqueous Mg concentration, due to precipitation of Mg-rich saponites.

Model C pursues a more realistic simulation of aqueous Mg, by deriving TST precipitation rates from the smectite dissolution rates determined by Ref. 51, (Abstract and p. 402). Three choices were tested for the effective surface area of the precipitating smectite.

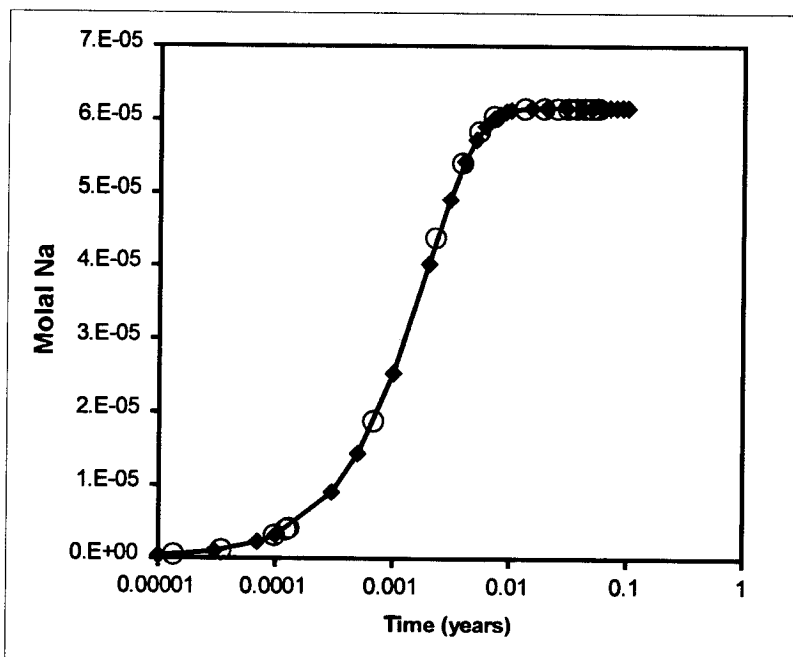
For Model C1, the baseline area was taken as the glass surface area. Micrographs of the corrosion crusts (e.g. Figure 2 in Ref. 20) show that the platy alteration minerals tend to grow with the plate surfaces roughly perpendicular to the glass surface, and the plate edges exposed sub-parallel to the glass surface. The input file for Model C1 was 'staine6s.6i'.

Model C2 uses a surface area of 1/5 the glass surface area, and is motivated by the observation of Turner and Pabalan (Ref. 71, p. 377) that the grain edges are the significant sorption sites on most clays. If the clay particles are oriented with the platy surfaces perpendicular to the glass surface, it is very unlikely that the edges will exceed the total surface area of the substrate (Turner and Pabalan suggest 10% of the total surface area is grain edges). The input file for Model C2 was 'stai_e6s.6i'.

On the other extreme, model C3 uses ten times the glass geometric surface area, and was chosen to assess the possibility that Huertas et al. (Ref. 51, p. 403) underestimated the activation energy (hence the 85.5 °C dissolution rate). The input file for Model C3 is 'stai!e6s.6i'.

6.3.1.3 Results: MCC-4 Models

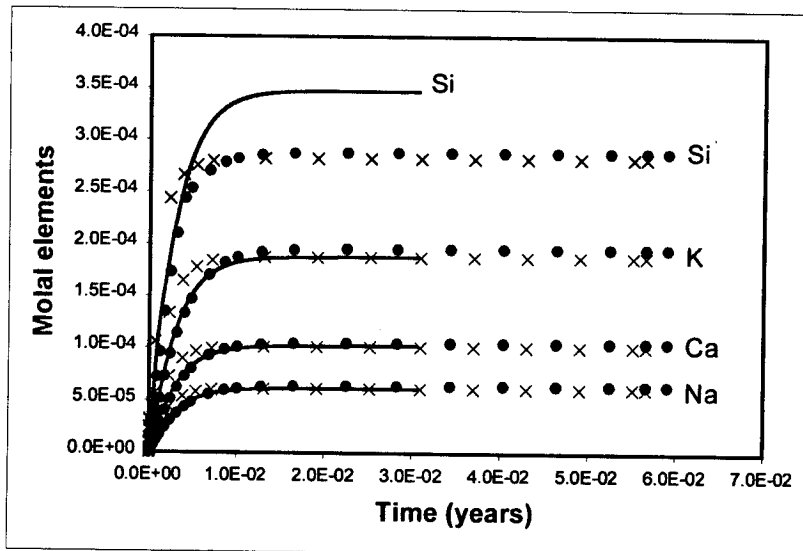
All models show an initial rise, followed by a plateau, for aqueous Na, K, Ca, Si and pH (Figure 6-5, Figure 6-3, and Figure 6-4); calculated in spreadsheet 'elem_stain00a_staine6a_stai_e6s.xls' (Attachment I). While Cooper and Cox (Ref. 20) refer to "initial and long-term" release rates, it is important to recognize that with the MCC-4 tests, the initial fast rise in concentration is largely unrelated to a change in the glass degradation mechanism.



The diamonds and continuous curve represent the analytical solution
Equation 3 and Equation 4;

The open circles show the results from MCC-4 Model A (file 'stain00A.6i').

Figure 6-3: Molal Na vs Time for Analytical Solution vs Model



Model A (x symbols), Model B (•) and Model C2 (solid line).

Figure 6-4: Predicted Si, K, Ca and Na Variations for MCC-4

Consider a model with a constant glass degradation rate, for elements such as Na and K (which are largely uninvolved in precipitation reactions, so long as the solutions are kept dilute by high flow rates). The aqueous molarity, is determined by the competition between glass dissolution and removal by flushing. The equation to describe the evolution of molarity, in such a system, is:

$$dM/dt = (S \cdot f \cdot k)/V - M \cdot (dV/dt)/V$$

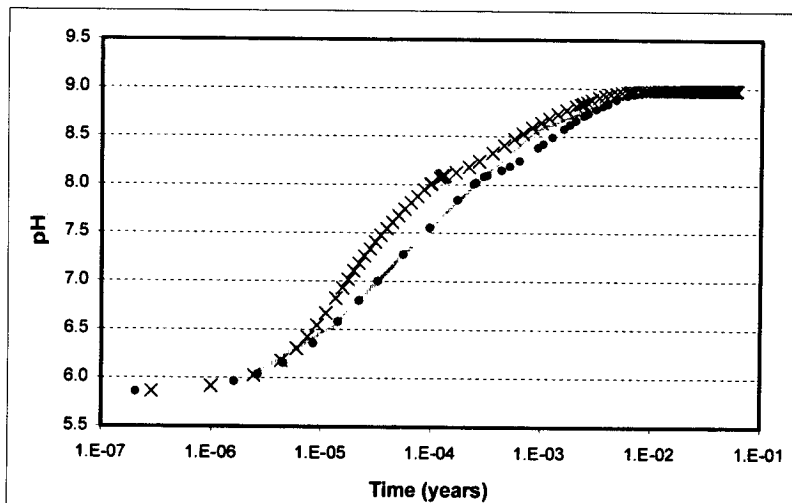
Equation 3

where t is time in seconds, S is the total surface area of the glass in cm^2 , f is the number of mols of the element per mol of glass, k is the dissolution rate in $(\text{mols glass})/(\text{cm}^2 \cdot \text{s})$, dV/dt is the rate of water flushing through the MCC-4 test (cm^3/s), and V is the test vessel volume in cm^3 . Equation 3 is derived by simple mass balance. For such dilute solutions, molarity is approximately equal to molality. It is easily verified, by substitution, that the solution to Equation 3 is:

$$M = ((S \cdot k \cdot f)/(dV/dt)) \cdot [1 - \exp(-(t \cdot dV/dt)/V)]$$

Equation 4

Thus there will be an initial rise in the aqueous concentration, followed by a plateau to $M = ((S \cdot k \cdot f)/(dV/dt))$ at long times, even though the glass corrosion rate is unchanging. Figure 6-3 compares Na concentrations predicted by Equation 4, to the results of Model A (EQ6 run 'stain00A.6i'). The excellent agreement indicates that the SCFT model in EQ6 is implemented correctly.



Model A (x symbols), Model B (•) and Model C2 (solid line)

Figure 6-5: Predicted pH Variations for MCC-4.

Figure 6-4 shows the predicted behavior of aqueous Na, Ca, K and Si. All models produce substantially similar results; the slight exception is the plateau Si content for Model C3, for which the aqueous Si is ~20% higher. For Model C2, the higher Si is due to the inhibition of Mg-smectite precipitation, which normally serves as a sink for silica. Figure 6-5 shows the evolution of pH for Models A, B and C. All models show a rapid rise to essentially the same pH (~9 at 85.5 °C). Because of the log time scale, Figure 6-5 emphasizes differences at early times; however, the various models produce nearly identical pH for the final 90% of the simulation time.

Figure 6-6 and Figure 6-7 show the predicted evolution of minerals assemblages (corrosion crusts) for Models A and C2, respectively. In both models, the dominant alteration phases are saponite (an Mg-smectite), apatite, and MnO₂, in molar proportions ~ 1 : 0.55 : 0.40. The observed minerals (Ref. 20) were Mg-smectite and apatite in the proportions ~ 1 : 0.33, with no explicit observation of MnO₂. However, in the Cox and Ford 1993 study, MnO₂ dendrites were observed in the corrosion crusts of similar glasses (Ref. 21, Figure 2 in original article). In the 1996 study, it may have been extremely difficult to identify an amorphous MnO₂ phase by the methods used. Cooper and Cox (Ref. 20, p. 513) characterize the smectite as Mg_(2-x)Mn_x[(Si_(4-y)Al_y)O₁₀](OH)₂·nH₂O, where x varies from 0 to 0.4 and y from 0.1 to 0.4; this formula requires the Mn be in the (IV) state for charge balance. Since Mn(IV)-smectites are not well-known, it seems possible that the clay observed by Cooper and Cox is actually an intergrowth of smectite and amorphous MnO₂. Thus, the agreement between the observed and predicted mineral assemblages is reasonably good.

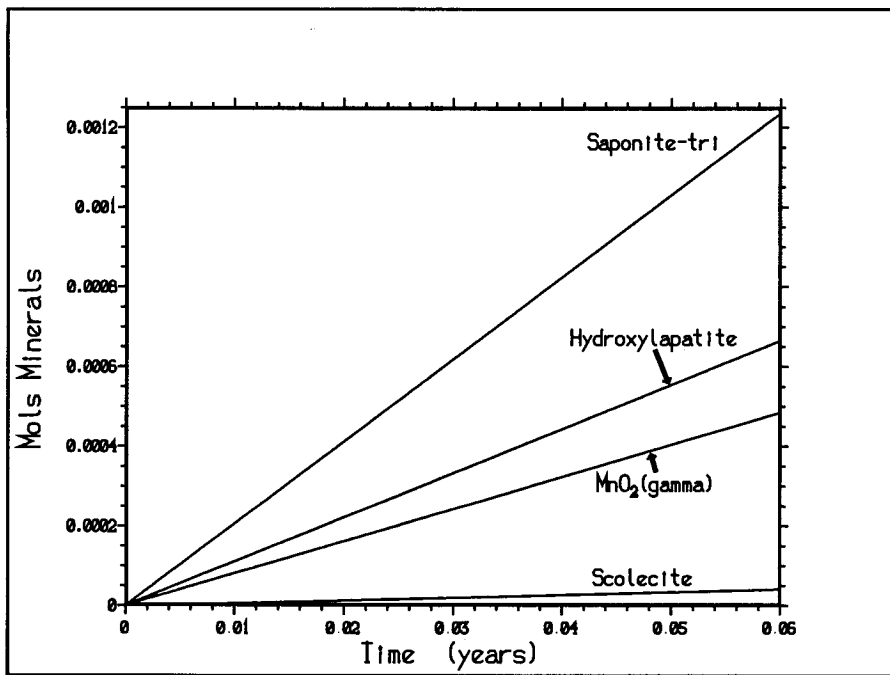


Figure 6-6: Corrosion Minerals Predicted for MCC-4 Model A

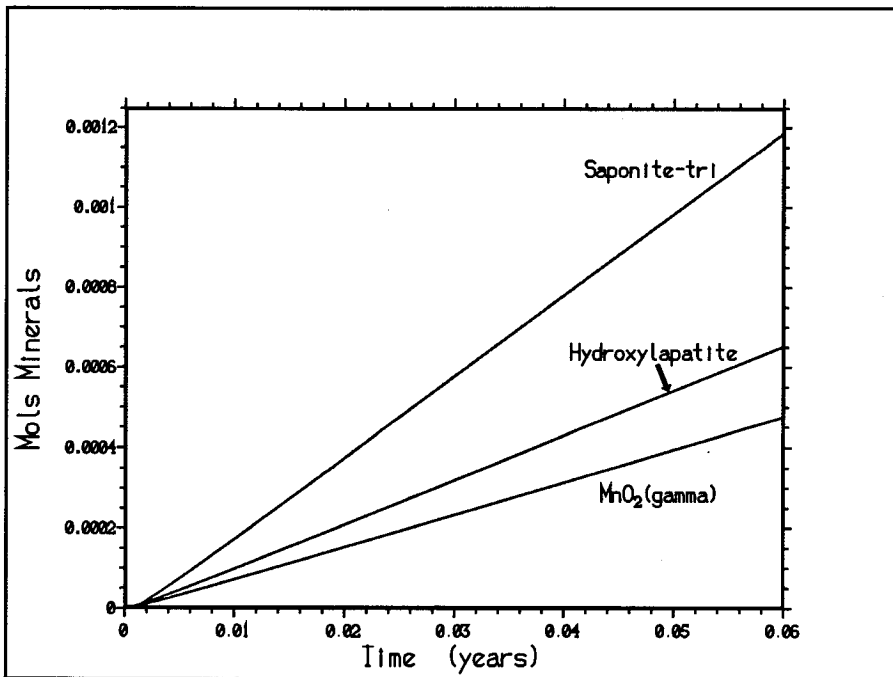
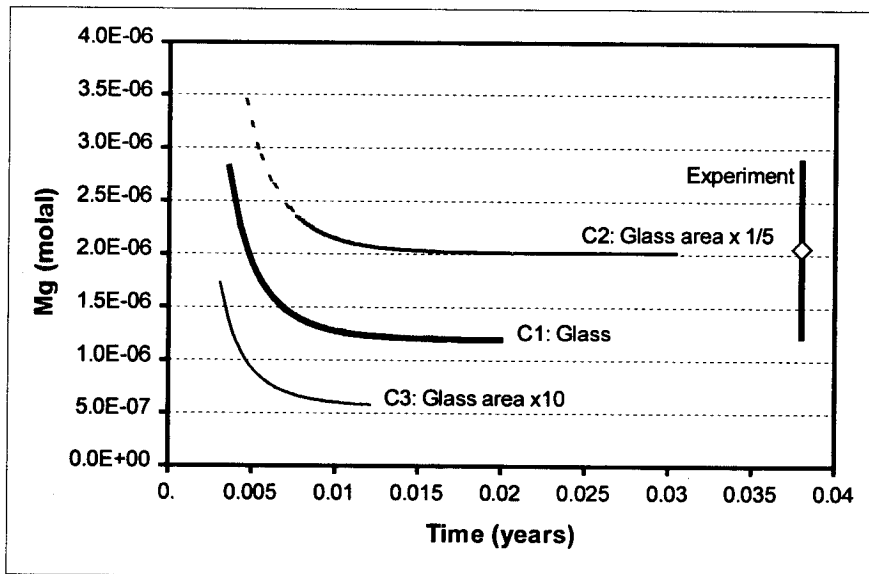


Figure 6-7: Corrosion Minerals Predicted for MCC-4 Model C2

The predicted volume of all corrosion products for Model C2, is 0.02148 cm^3 . The observed crust thickness is 10 to 40 microns, corresponding to 0.00450 to 0.01800 cm^3 , with an average of 0.01125 . Thus, the model predicts roughly twice the “average” observed volume. Given the

approximate nature of the observed thicknesses, and the uncertainty in the rates and effective surface areas, this agreement is considered reasonably good.



Note: Spreadsheet 'Mg_stain_glass_expt.xls'.

Figure 6-8: Experimentally Observed (error bar) Aqueous Mg Concentrations, and Concentrations Predicted for Models C1, C2 and C3

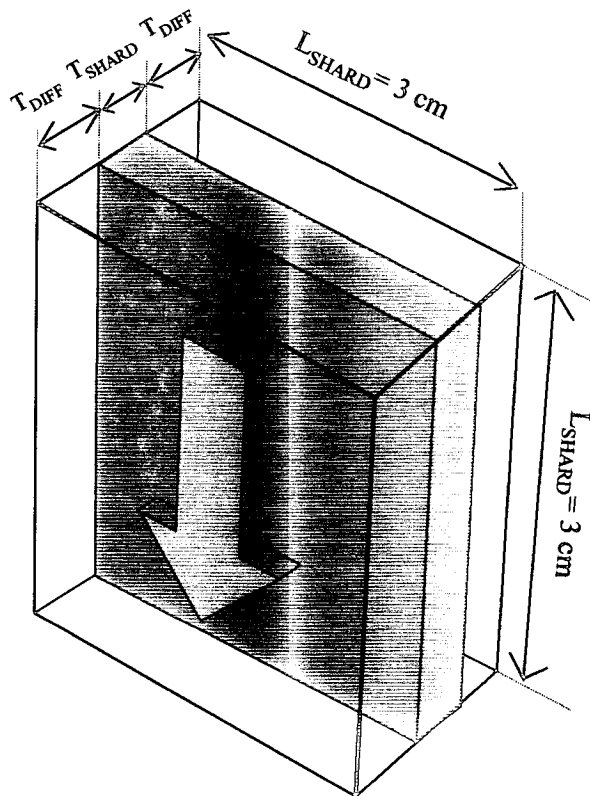
Figure 6-8 gives the Mg concentrations observed in the MCC-4 test (at steady-state), and the concentrations predicted by Models C1, C2 and C3. Despite the 50-fold variation in the surface area used in the models, the plateau Mg concentration varies by just a factor of four. The C2 Model predicts Mg concentrations close to the observed mean, and the C1 Model is just outside the observed Mg concentration range. The agreement between the models and observation is good, given the uncertainties in the effective surface areas, rates, and the approximation inherent in deriving a TST precipitation law from dissolution studies.

6.3.1.4 Methods: Archeological Models

The degradation of glass shards in soil, for up to 320 years, was modeled in a two-step process. First, water was equilibrated at 25 °C with illite and calcite at $fO_2=0.2$, based on the observations that the Yorkshire soils contain clays and limestones (Ref. 53, p. 325), and that calcite is observed within or adjacent to the altered glass (Ref. 20, p. 513). The CO_2 fugacity of this initial solution was varied until the equilibrium pH matched the observed soil pH of 7.6 (Ref. 19, p. 525). The final fCO_2 was $\sim 10^{-2.22}$. The input files for the process were 'clay!h2o.3i' and 'clay!h2o.6i' (folder 'glass' in Attachment I). The solids were removed from this fluid, and the fluid (hereafter called "soil water") was used as a "displacer" reactant in the second stage of the model. The second stage represents the flow of soil water past a buried glass shard; the fCO_2 and fO_2 were not fixed in the second stage, but were controlled by the gases dissolved in the soil water, and the interaction with the degrading glass.

Two variations on the archeological model (hereafter called I and II) were considered. Model I

is intended to represent a glass shard in an environment that washes the surface efficiently, via the downward flux of water from rainfall. The input file for Model I was 'gla!cly0.6i'. For the EQ6 simulation, the aqueous volume around the shard is defined by the shard length and width, and by the effective diffusion thickness (calculated in spreadsheet 'glass_archeol.xls', sheet 'comp&size'; Figure 6-9).



NOTE: Flow of soil water is in the direction of the large arrow. The thickness of the diffusion zone (T_{DIFF}) is defined in spreadsheet 'glass_archeol.xls'. The shard length is L_{SHARD} , and the fluid volume for the EQ6 calculation is $2 \cdot L_{\text{SHARD}} \cdot T_{\text{DIFF}}$.

Figure 6-9: Geometry for Archeological Glass Corrosion Models I and II

The diffusion thickness is the approximate distance solutes would diffuse into the surrounding porous soil, during the length of time it would take a packet of recharge water to flow the length of the shard. The recharge rate is taken as 100 cm/year; this is an upper estimate, exceeding the observed average precipitation rate of 90.6 cm/yr for the Upper Yorkshire catchment basin (Ref. 53, p. 325). (Rainfall provides an overestimate of true recharge, because some of the precipitation is lost to evaporation and uptake by plant roots. Moreover, in a clay-rich soil, there may be regions of very low permeability, and locally low fluence of water.) With the dimensions of the EQ6 volume, the presumed recharge rate defines a flux of soil water into the system. Model I is not intended to be a realistic depiction of the soil water system, but a plausible upper bound on the flushing experienced by the glass shards. Model II is identical to Model I, except the total flux of soil water through the system is dropped by a factor of ten, to

represent a system with more limited flushing, such that the fluid near the glass surface will have a higher probability of accumulating alkali metals from glass degradation. Model I was run out to 65 years, at which point the calculation reached a steady-state, and iteration became prohibitively slow. Model II was run to 320 years, again limited by the decreasing size of the EQ6 time steps. The input file for Model II was 'gla!cly2.6i'.

6.3.1.5 Results: Archeological Models

The difference in behavior, between the two models, is striking, and provides a simple explanation for the observation of Cooper and Cox (Ref. 20) that the soil glass appeared to have corroded more rapidly than would be predicted by the MCC-4 experiments.

Figure 6-10 and Figure 6-11 show the pH, and amount of glass remaining, for Models I and II. For Model I, the pH plateaus at 7.84, only slightly above the initial soil water value of 7.6, and the glass degradation rate is sufficiently slow to ensure that some of the shard will remain at the end of 450 years. In Model II, the pH rapidly reaches a plateau of 11.1, which greatly increases the degradation rate, so that no glass remains after ~26 years. The high pH is achieved by two factors. First, the lower flushing rate allows more alkali to build up near the surface of the shard, which raises the pH; and in turn, the increased pH further increases the degradation rate (via Equation 2), producing a positive feedback. Thus, the speculation of Cooper and Cox (Ref. 20, p. 518) that in the soils, "the pH at the glass surface may be very high" appears justified.

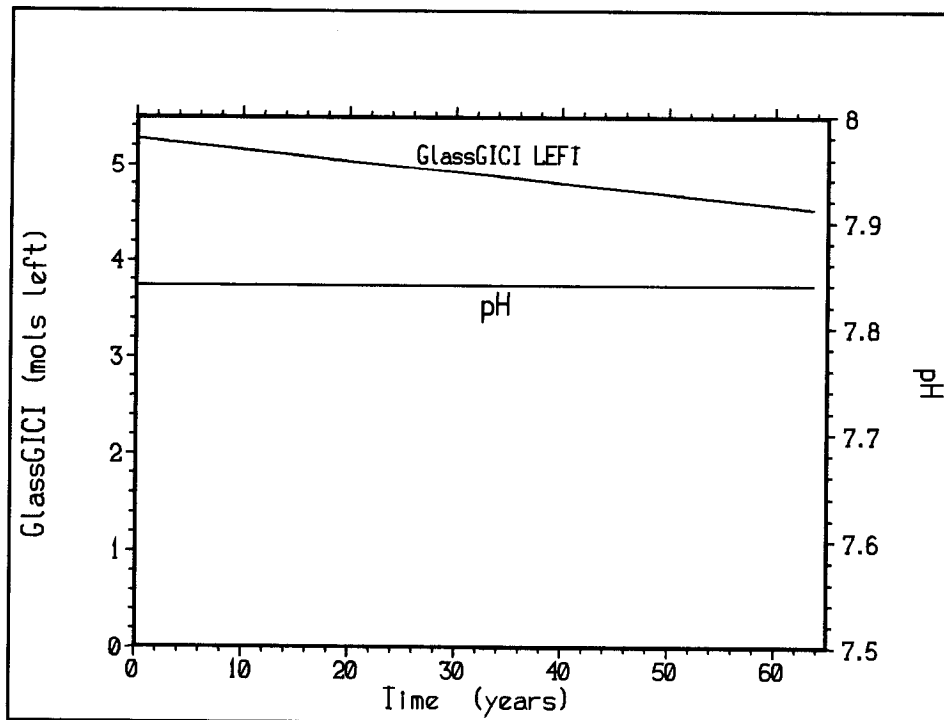


Figure 6-10: pH and Glass Consumption for In-Soil Corrosion Model, Model I

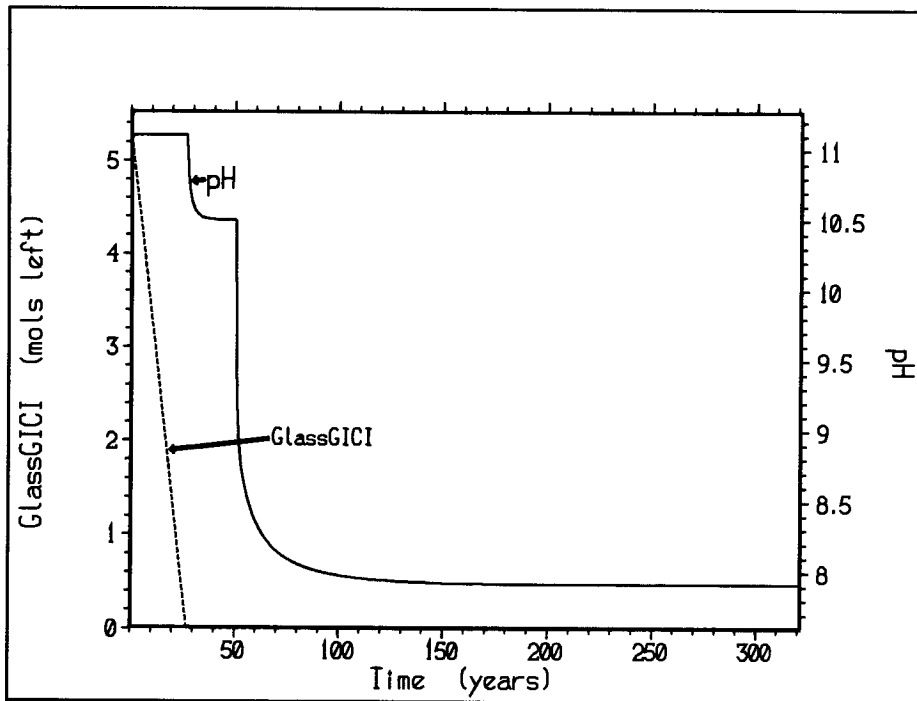


Figure 6-11: pH and Glass Consumption for In-Soil Corrosion Model, Flow Rate Dropped by 10x, Model II

Figure 6-12 and Figure 6-13 show the minerals predicted for Models I and II. In both models, calcite (CaCO_3), silica (here modeled as chalcedony, or cryptocrystalline quartz), apatite and MnO_2 dominate. For the archeological corrosion crusts, the observed phases are: a porous silica “gel,” Ca-phosphate, CaCO_3 and MnO_2 . Thus if the chalcedony is associated with the porous silica “gel,” the match between model and observation is quite good. Presumably, silica gel is a thermodynamically less stable than chalcedony; however, the “gel” may be stabilized, relative to chalcedony, by residual alkali (Ref. 41, pp. 345-346).

6.3.2 Summary of Glass Modeling

The MCC-4 and archeological models meet the proposed metrics. The MCC-4 models match the types and amounts of experimentally observed phases, given the uncertainties in the experiments and the subsequent chemical analyses. The aqueous Mg concentration is matched with varying success, depending on the estimate of surface area. For the two lower surface areas, Mg concentrations either match well, or nearly within the experimental uncertainty; while for the highest surface area, the predicted values are $\sim 1/4^{\text{th}}$ the observed value. Given the factor 50 rate variation implicit in this test, the overall match is considered good. The archeological model provides a plausible explanation for the accelerated dissolution rates (local high pH from slow rates of recharge), and also matches the product phase assemblages.

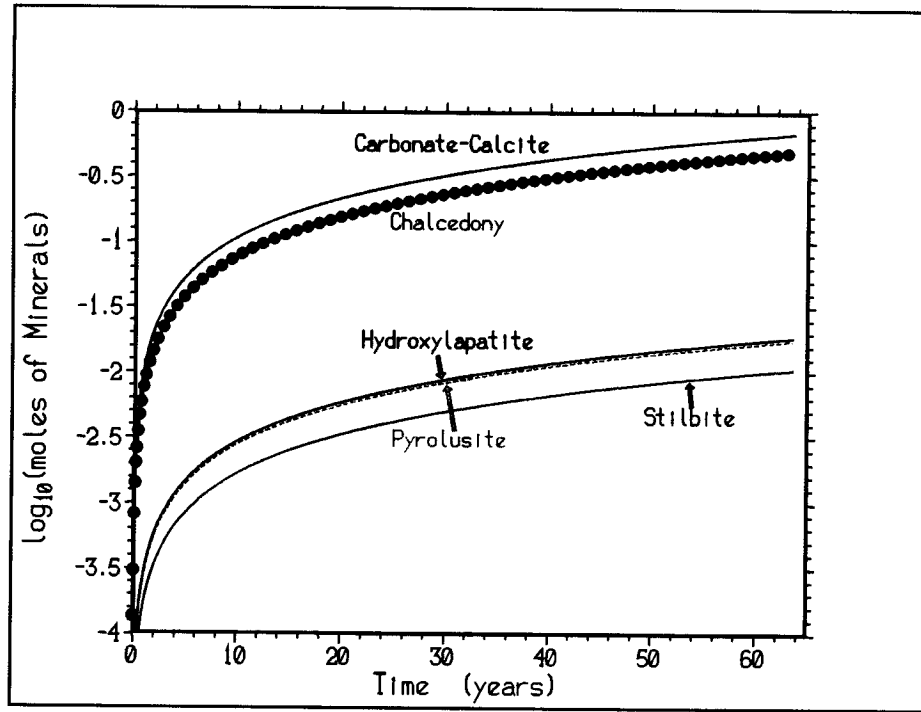


Figure 6-12: Minerals Predicted for In-Soil Corrosion Model, Model I

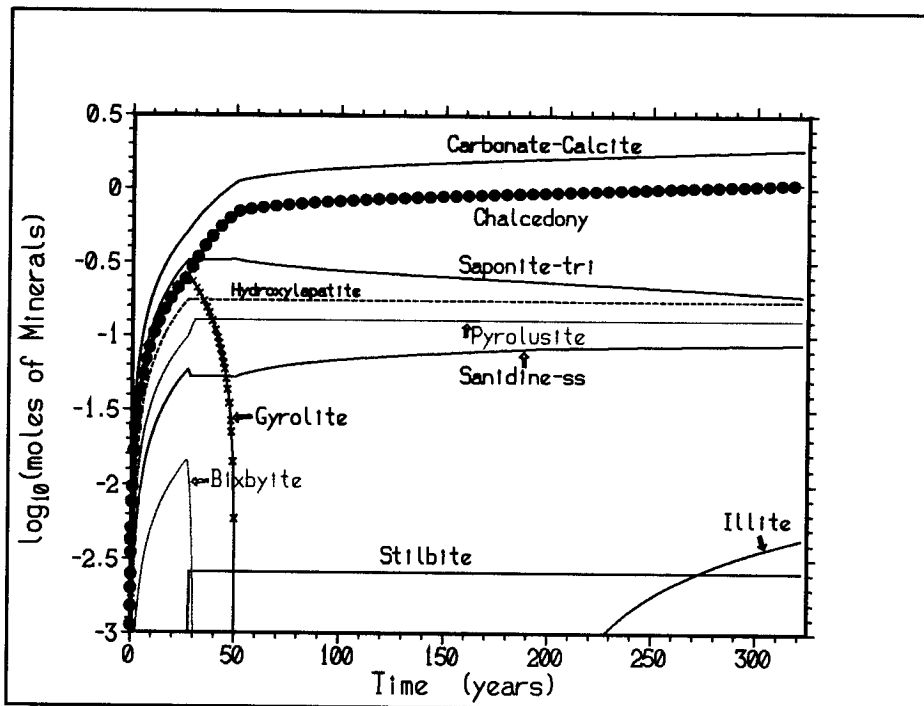


Figure 6-13: Minerals Predicted for In-Soil Corrosion Model, Flow Rate Dropped by 10x, Model II

6.3.3 Fuel Degradation Sub-Model

The fuel degradation sub-model can be validated by comparison with laboratory experiments. In particular, confidence in the model is increased if the model predicts the minerals formed in the experiments, and also predicts some quantitative aspect of the experimental chemistry, such as aqueous concentrations of actinides. To be suitable for such a comparison, the experiments must meet the following conditions:

- (1) Thermodynamic data must be available, or easily extrapolated, for the experimental conditions. In the current, qualified EQ6 database Ref. 59, thermodynamic data for most actinide solids and aqueous species are limited to 25°C. Thus it is necessary to use experiments conducted at low temperature.
- (2) The experimental work should provide chemical composition, the amount, total surface area, and the rate of degradation for each component, so that a quantitative model can be constructed.
- (3) The experiments should involve materials and conditions similar to those expected in the WP; these conditions include the composition of the in-dripping aqueous phase.
- (4) The experiment should be of as long duration as possible, to increase confidence in the extrapolation to the time scales of WP degradation.

The HBR-3-25 experiments of Wilson (Ref. 75) and Wilson and Bruton (Ref. 76) were chosen for validation of the EQ6 fuel degradation sub-model. These experiments meet the criteria outlined above; the tests were conducted at 25°C, the solutions were analyzed periodically for actinide concentration, the material used was an actual spent fuel in J-13 water, in a stainless-steel vessel; and the tests were run for up to a year. The radiation environment was undoubtedly more severe in the experiments, than would be expected for a WP breached after 10^4 years, since the spent fuel used in the experiments contained significant activity of short-lived fission products.

6.3.3.1 Preliminary Fuel Model 1 and PuO₂ Solubility Sensitivity

Fuel Model 1 is based on the calculations provided by Wilson and Bruton (Ref. 76). The template for the Fuel Model 1 is the standard EQ6 test file 'j13wsf.6i' (Ref. 77, p. 297, called 'j13wwsf.6i' in original manual). This test file simulates the reaction of 100 g of spent UO₂ fuel into 1000 g J-13-like water at $\log_{10}(f(\text{CO}_2)) = -3.5$. Fuel Model 1 differs from the original Wilson and Bruton calculations in two ways: (1) Fuel Model 1 uses the qualified 'data0.ymp' database, vs. the older data0.com used by Wilson and Bruton, and (2) Fuel Model 1 uses the "closed system" option, as opposed to the "titration" option, to ensure that the calculation runs until all the fuel is reacted and near-steady-state aqueous concentrations are achieved. The Fuel Model 1 input file is denoted 'j13wsf_.6i' and is located in folder 'j13wsf'.

Figure 6-14 compares the experimentally measured Pu concentrations with the EQ6 predictions of Fuel Model 1 (indicated by 'data0.ymp'), and the EQ6 predictions of Wilson and Bruton. Wilson and Bruton give two values, based on the assumptions of equilibrium with amorphous Pu(OH)₄ versus equilibrium with crystalline PuO₂. Clearly, the Fuel Model 1 predictions are much closer to the experimental results, than are the original Wilson and Bruton predictions. The better match is due principally to the updated thermodynamic data for PuO₂. However, the Fuel Model 1 result is still ~ 1.3 orders higher than the experimental observations. To better

match the experimental values, the stability constant in the thermodynamic database, logK, for PuO₂ was reduced by 1.3 units, via the EQ6 “augmentk” input file parameter (folder ‘j13wsf’, file ‘j13wsf13.6i’). Not surprisingly, the result is a close match between the predicted Pu concentrations with the experimental values (folder ‘j13wsf’, file ‘j13wsf.xls’). Figure 6-14 shows the “augmentk=-1.3” line matches exactly with the experimental value.

Using Pu concentrations that are higher than expected is conservative for external criticality concern, but not conservative for internal criticality concerns. To determine the sensitivity to the value of the logK for PuO₂ on losses from the waste package, a case from a recent calculation (Ref. 15, Case s10) was rerun, using the database as it is (‘data0.yme’) and using a PuO₂ logK value that was lowered by 1.3. The cumulative losses of Gd, Pu, and U were calculated (folder ‘j13wsf’, file ‘j13wsf.xls’) and are listed in Table 6-11. The loss of Pu and U was only slightly higher for the case that uses the ‘data0.yme’ database.

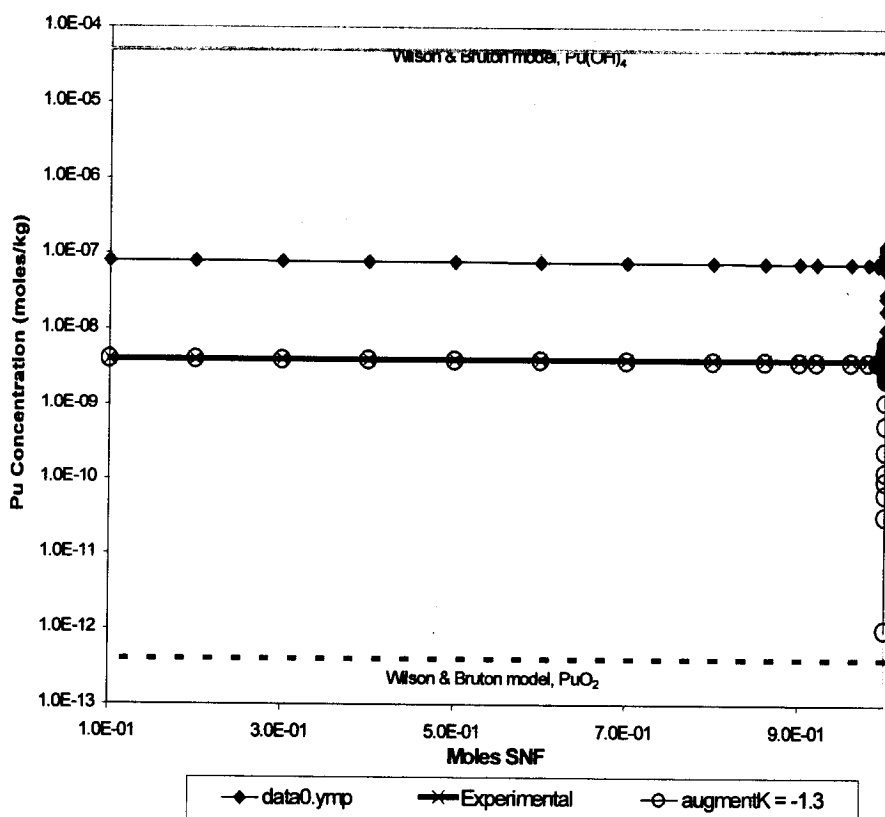


Figure 6-14. Simulated Versus Experimental Pu Concentration

Table 6-11. Comparison of Results with Reduced PuO₂ LogK Values

Case ID	Root Name	LogK PuO ₂	Years	%Gd Loss ^a	%Pu & U Loss
s10	p52_L142	-4.2197 (‘data0.yme’)	2.22E+04	53.35	0.45
s10a	p52aL142	-5.5197 (augmentk = -1.3)	2.22E+04	53.36	0.39

For aqueous uranium, the agreement between experiments and the Fuel Model 1 is significantly worse. Fuel Model 1 predicts an aqueous U concentration of $\sim 10^{-4}$ M. For cycle 3 of HBR-3-25 (the “cleanest” subset of the experiment, in which the high-surface area fines had been removed), the observed aqueous U is $\sim 10^{-6}$ M, two orders of magnitude lower. However, there are obvious limitations in Fuel Model 1. First, the model is non-kinetic. Given the limited amount of silica in the J-13 water, the long-term U concentration will always rise to a level determined by schoepite ($\text{UO}_3 \cdot n\text{H}_2\text{O}$) once all the silica is consumed. Second, the Wilson and Bruton model fixes the fugacities of O₂ and CO₂ to ambient values, while the series 2 experiments were nominally capped, and the series 3 experiments were definitely closed. The dominant aqueous U species, predicted by Fuel Model 1, are $(\text{UO}_2)_2\text{CO}_3(\text{OH})_2$, $\text{UO}_2(\text{CO}_3)_2^{2-}$ and $\text{UO}_2(\text{CO}_3)_3^{4-}$. The equilibrium constants (K_s) for these species depend on the carbonate concentration raised to the first, second and third powers, respectively, so the U solubility is fairly sensitive to the assumptions about CO₂ control. (In contrast to the Wilson and Bruton experiments, the WP degradation models are inherently open to the atmosphere, thus it is more reasonable to model the WPs with fixed CO₂ fugacities.) The following section discusses refinements to the basic Wilson and Bruton model.

6.3.3.2 Degradation Fuel Model 2

Fuel Model 1 (Section 6.3.3.1) can be refined by using kinetic degradation rates, and by implementing more realistic controls on the O₂ and CO₂ fugacities. Fuel Model 2, developed in this section, is a more detailed simulation of cycle 3 of the HBR-3-25 test, as described by Wilson (Ref. 75).

Test HBR-3-25 employed bare (clad removed) SNF fuel in a sealed 304 stainless steel container at 25°C. Cycle 3 of this test was analyzed by Steward (Ref. 32, Table 28), who derived specific surface areas and degradation rates. After the reaction vessel was filled, the test was closed to the atmosphere, and involved 80.7g of fuel in 250 cm³ of J-13 water. The EQ6 simulation did not buffer the fO₂ or fCO₂, but allowed the gas fugacities to drift; in contrast, Wilson and Bruton (Ref. 76) chose to fix gas fugacities to the atmospheric ambient. The details of the EQ6 simulation, including the fuel composition (molar), degradation rate (moles/cm²-s), geometric surface area (cm²/g), and moles of O₂ and CO₂ in the headspace are explained in file ‘j13fuel_081001.xls’, in folder ‘Fuel2’ (Attachment I). The EQ6 simulation was run for 1.0 year. Two versions of Fuel Model 2 were run. Fuel Model 2A ignored the stainless steel container (input filename: ‘j13fuel.6i’), used for the HBR-3-25 test, whereas Fuel Model 2B included the steel liner of the vessel (input filename: ‘j13sfuel.6i’).

Figure 6-15 and Figure 6-16, respectively, show the concentration of radionuclides in solution

and the mineral assemblage, as predicted by Fuel Model 2A. The sequence of U minerals, formed from the reaction of J-13 with the corroding fuel, begins with formation of alpha-uranophane ($\text{Ca}(\text{UO}_2\text{SiO}_3\text{OH})_2\cdot\text{H}_2\text{O}$), followed by boltwoodite ($\text{NaUO}_2\text{SiO}_3\text{OH}\cdot1.5\text{H}_2\text{O}$) and schoepite ($\text{UO}_3\cdot\text{nH}_2\text{O}$). The mineralization sequence appears to follow an increase in the ratio of uranium to silicate, reflecting a decrease in concentration of silica in J-13 water.

Wilson reports the results of instrumental analysis with a Scanning Electron Microscope (SEM) equipped with an Energy Dispersive X-Ray (EDX) unit for semi-quantitative analysis of alteration-product compositions. In addition, powder X-Ray Diffraction (XRD) was performed on selected runs. The EDX spectrum (Figure 4 of Ref. 75) identified a calcium-uranium-silicate composition. The XRD patterns of the same test at higher temperature (HBR-3-85) identified uranophane and tentatively, haiweeite. In addition, precipitated silica and calcite flakes were also identified on several of the filters. Examining Figure 6-16 of the EQ6 simulation for the same period as the experiments reveals similar mineralization patterns, with formation of uranophane as the major uranosilicate mineral, and both precipitation and dissolution of calcite and chalcedony. This comparison shows reasonably good agreement between the experiments and Fuel Model 2A. Haiweeite is not predicted in Fuel Model 2A, simply because there is no entry for Haiweeite in the thermodynamic database ('data0.ymp', Ref. 59). Nonetheless, only very small quantities of haiweeite were observed in the experiments.

Quantitatively, U and Pu concentrations reported by Wilson were 0.3-0.4 $\mu\text{g}/\text{ml}$ for U (Figure 6-17, cycle 3, HBR 3-25) and 80-100 pCi/ml for Pu. Wilson provides a conversion factor of $1.0\text{ng Pu}/\text{ml} = 100 \text{ pCi}/\text{ml}$ for Pu that corresponds to a concentration of 0.8-1.0 $\text{ng Pu}/\text{ml}$. Conversion to molality allows a comparison of the results obtained by EQ6 simulations to those reported by Wilson. The conversion of U concentration reported by Wilson is:

$$0.3 \frac{\mu\text{g of U}}{\text{ml soln}} \times \frac{1000\text{ml soln}}{1\text{L soln}} \times \frac{1\text{L soln}}{\text{kg soln}} \times \frac{1\text{g soln}}{10^6 \mu\text{g soln}} \times \frac{1 \text{ mole U}}{238 \text{ g of U}} = 1.26 \cdot 10^{-6} \frac{\text{moles U}}{\text{kg soln}}$$

A concentration of 0.4 $\mu\text{g U}/\text{ml}$ results in a concentration of $1.68 \cdot 10^{-6}$ moles U/kg soln. In comparison, Fuel Model 2A predicts a concentration of $1.66 \cdot 10^{-6}$ moles U/kg soln (inverse log of -5.78, Figure 6-15) which is in excellent agreement with the results obtained by Wilson.

The conversion of Pu concentration reported by Wilson is:

$$0.1 \frac{\text{ng of Pu}}{\text{ml soln}} \times \frac{1000\text{ml soln}}{1\text{L of soln}} \times \frac{1\text{L soln}}{\text{kg soln}} \times \frac{1\text{g soln}}{10^9 \text{ng soln}} \times \frac{1 \text{ mole Pu}}{244 \text{ g of Pu}} = 4.1 \cdot 10^{-9} \frac{\text{moles Pu}}{\text{kg soln}}$$

EQ6 simulation predicts a concentration of $8.91 \cdot 10^{-8}$ moles Pu/kg soln (inverse log of -7.05, Figure 6-15). The agreement is within a factor of 5, which is significantly better than the factor 20 difference seen in Fuel Model 1. In addition, it must be considered that in the Wilson experiment, all samples were passed through a $0.45 \mu\text{m}$ filter before chemical analysis. Dissolved Pu species have a high tendency to adsorb to suspended and colloidal particles in solution. In the UZ flow and transport PMR (Ref. 37) maximum and minimum K_d values for a number of elements are reported as function of rock type and main WP corrosion products (Iron Oxides) in the UZ units. Information in Table 6-12 was obtained from Ref. 37 (Table 3.11-1, p. 236). The reported K_d values reveal that Pu has a much higher sorptive properties than U. This

could contribute to higher concentration of Pu observed in simulation compared to the experimental results.

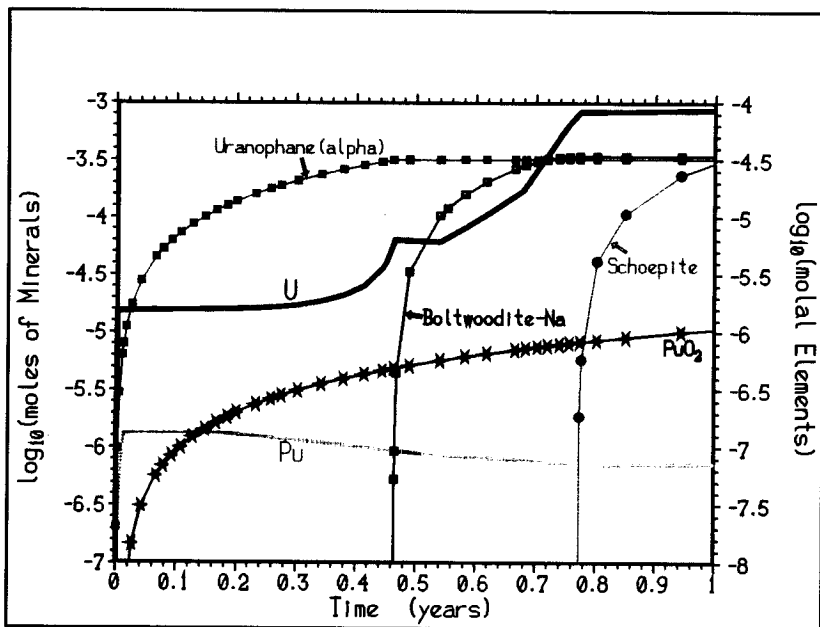


Figure 6-15: Fuel Model 2A. Concentration of Radionuclide Elements and Minerals vs. Time

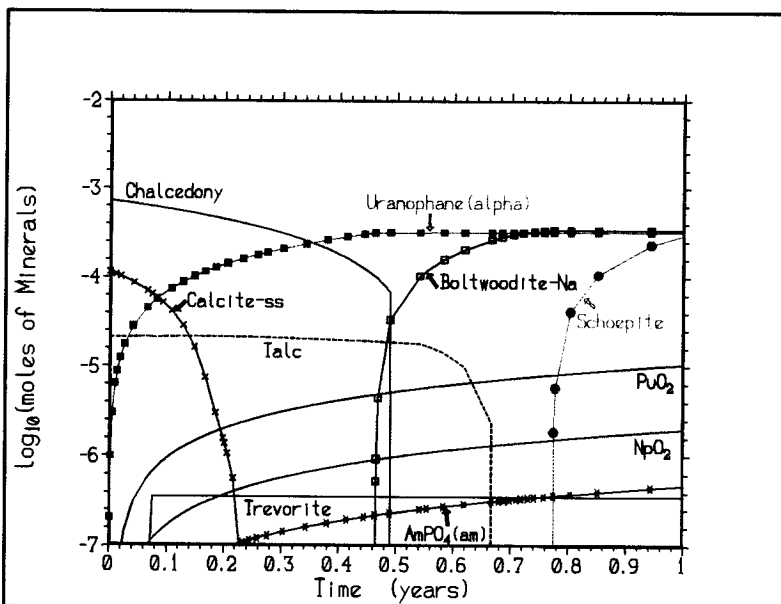


Figure 6-16: Fuel Model 2A. Moles of Minerals and Aqueous Concentrations of Pu and U vs. Time

Table 6-12: Sorption Coefficient Distributions for UZ Unite

Element	Rock type	Min Kd (mL/g)	Max Kd (mL/g)
Pu	Devitrified	5	70
	Vitric	30	200
	Zeolitic	30	200
	Iron Oxide	1000	5000
U	Devitrified	0	2
	Vitric	0	1
	Zeolitic	0	10
	Iron Oxide	100	1000

Source: Adapted from Ref. 37

Figure 6-18 shows the results of Fuel Model 2B, in which the stainless steel was allowed to corrode. The aqueous concentrations and the mineral sequences are virtually identical to those in Figure 6-15, which indicates that stainless steel had a negligible effect on the modeling.

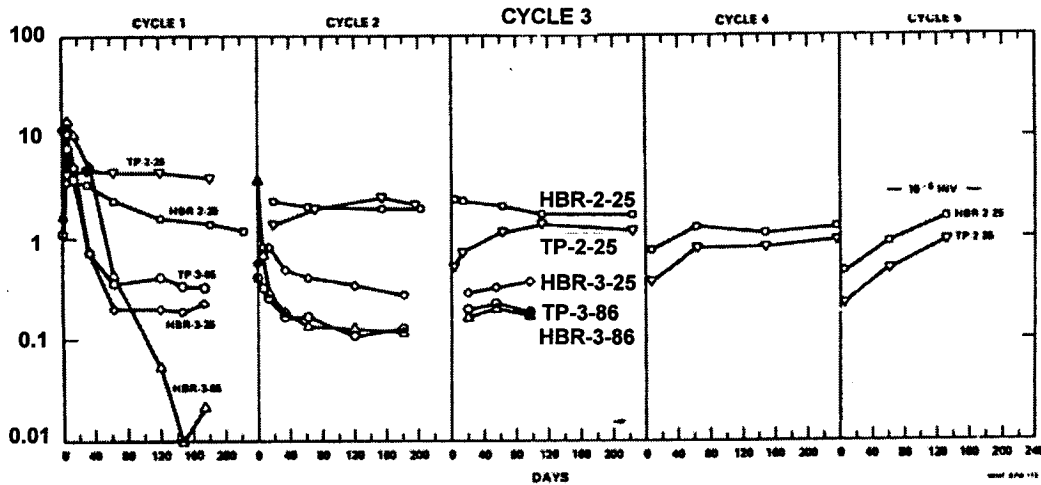


Figure 6-17: Uranium Concentration Measured in 0.4 μm Filtered Solution Sample (Wilson, Figure 2)

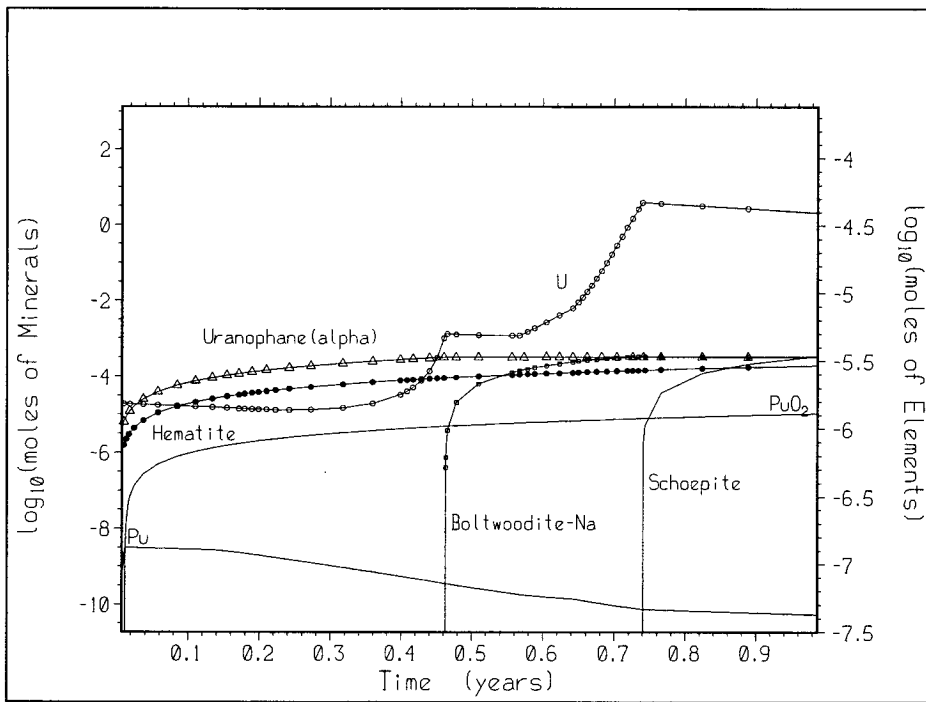


Figure 6-18: Fuel Model 2B, Moles of Minerals and Aqueous Concentrations of Pu and U vs. Time

6.3.4 Solubility-Limiting Uranium Phases in Mixed Glass/Fuel Systems

EQ6 simulations for degradation of codisposal packages typically predict a sequence of uranium alteration phases with relatively low Si/U. Such phases include schoepite ($\text{UO}_3 \cdot \text{nH}_2\text{O}$), soddyite ($(\text{UO}_2)_2\text{SiO}_4 \cdot 2\text{H}_2\text{O}$), uranophane ($\text{Ca}(\text{UO}_2\text{SiO}_3\text{OH})_2 \cdot 5\text{H}_2\text{O}$), and boltwoodite ($\text{NaUO}_2\text{SiO}_3\text{OH} \cdot 1.5\text{H}_2\text{O}$), with molar Si/U ratios ranging from 0 to 1. In contrast, experimental degradation of actinide-bearing waste glasses tends to produce weeksite ($\text{Na}_2(\text{UO}_2)_2\text{Si}_5\text{O}_{13} \cdot 3\text{H}_2\text{O}$, with Si/U = 2.5) as the dominant U-bearing phase, along with lesser amounts of uranophane and haiweeite ($\text{Ca}(\text{UO}_2)_2(\text{Si}_2\text{O}_5)_3 \cdot 5\text{H}_2\text{O}$, Si/U=3) (Ref. 55, p. 128). It is expected that both glass and actinide ceramics may degrade simultaneously in the WPs, so it is important to understand the apparent contradiction between predicted and observed uranium solids.

There are reasonable explanations for the discrepancy. The experiments that yield weeksite and haiweeite may have much higher silica concentrations, than are predicted for the codisposal WPs. Indeed, degradation of alkaline glass often produces an amorphous silica layer (Ref. 20), suggesting very high silica activity. However, The degraded WPs contain abundant steel corrosion products, which would be expected, through long times, to react with the corroded glass to form relatively Si-poor nontronite clays. In addition, the experiments are typically run at temperatures near 90 °C; whereas the WP models are constrained, in part by lack of thermodynamic data for U phases, to 25 °C.

It is hypothesized that the discrepancy in U solids is due principally to the controls on Si activity in the degrading glass, vs. the WP. To test this hypothesis, an FFTF (Ref. 65) model was altered to remove the steels that would potentially react with silica.

6.3.4.1 EQ6 File Inputs

This EQ6 simulation consisted of MOX and UOX fuel and HLW glass. The parameters for the input file are described in Table 6-13 and Table 6-14.

Table 6-13. Properties of Reactants

	MOX ^a		UOX ^a		HLW Glass ^b			
Total Moles of Reactant	0.39378 ^c		0.0182 ^c		24.821 ^c			
Chemical Composition	O	7.397063E-01	O	7.406648E-01	O	2.7039E+00	Si	7.7649E-01
	U	2.746725E-01	U	3.703324E-01	U	7.8186E-03	B	2.9124E-01
	Pu	9.407909E-02			Ba	1.0751E-03	F	1.6615E-03
	Np	1.101603E-03			Al	8.6298E-02	Fe	1.7221E-01
Surface Area (cm²)	1559.383 ^c		72.0726 ^c		1340.6 ^c			
Reaction Rate (mol/cm²·s)	1.1422E-14 ^d		1.1422E-14 ^d		1.3541E-10 (cdac 0.6) ^e 1.0756E-17 (cdac -0.4) ^e			

Sources: ^a The MOX and UOX chemical composition comes from 'Glass&Fuel' (Ref. 65).

^b The glass chemical composition is based on Ref. 28 (Attachment I, p. I-7) as simplified in 'HLW_glass REV01.xls', sheet 'composition' (Attachment I). This is the composition added to 'data0.yme' (in Attachment I) for the mineral, GlassSRL.

^c The number of total moles of reactants and surface areas come from DTN: SN9911T0811199.003: 'ffff_fuel_hws_rev04.xls', sheets 'Mols_rct'

^d The Fuel rate comes from Ref. 65, converted in 'FFTF IA 2001.xls', sheet 'MOX,UOX' (Attachment I)

^e The HLW Glass: (Ref. 39) Eq. 7 and 8, converted to EQ6 format in 'HLW_glass REV01.xls', sheet 'rates' (Attachment I).

Table 6-14. EQ6 Input File Elemental Molal Composition for J-13 Well Water

Chemical Composition							
O	5.55E+01	Gd	1.00E-16	Na	1.99E-03		
Al	1.00E-16	H	1.11E+02	Ni	1.00E-16		
B	1.00E-16	C	2.07E-03	Np	1.00E-16		
Ba	1.00E-16	P	1.00E-16	Pu	1.00E-16		
Ca	3.24E-04	K	1.29E-04	S	1.92E-04		
Cl	2.01E-04	Mg	8.27E-05	Si	1.02E-03		
Cr	1.00E-16	Mn	1.00E-16	U	1.00E-16		
F	1.15E-04	Mo	1.00E-16				
Fe	1.00E-16	N	1.42E-04				
Drip Rate (m ³ /year) ^a		Drip Rate (normalized for EQ6 input) (moles/sec) ^b					
0.15		8.18545E-10					

Sources: from Ref. 40 (Table 6), based on Ref. 58. These values are outputs from EQ3NR for input into EQ6 input file.

Notes: Drip rate selection is explained in Ref. 26 (Section 5.1.1.3), and were converted from m³/yr to moles/sec for input into EQ6 in the 'Rates' tab of 'fftf_fuel_hws_rev4.xls' DTN: SN9911T0811199.003 (Ref. 65).

Several minerals are routinely suppressed (not allowed to form) in most EQ6 runs, including the runs for this study. These minerals are listed and explained in Section 6.2.5.

6.3.4.2 Method

First, a run was completed suppressing only the default minerals listed in Section 6.2.5. Weeksite did not form. The Si minerals that did form were noted, and those minerals with the lowest LogK value were suppressed one at a time in successive runs. For each run, the minerals that formed and the Log(Q/K)(saturation state) were plotted (Figure 6-19 through Figure 6-22). The Log(Q/K) for weeksite gets closer to 0 (and thus becoming more likely to form), as each Si mineral is suppressed.

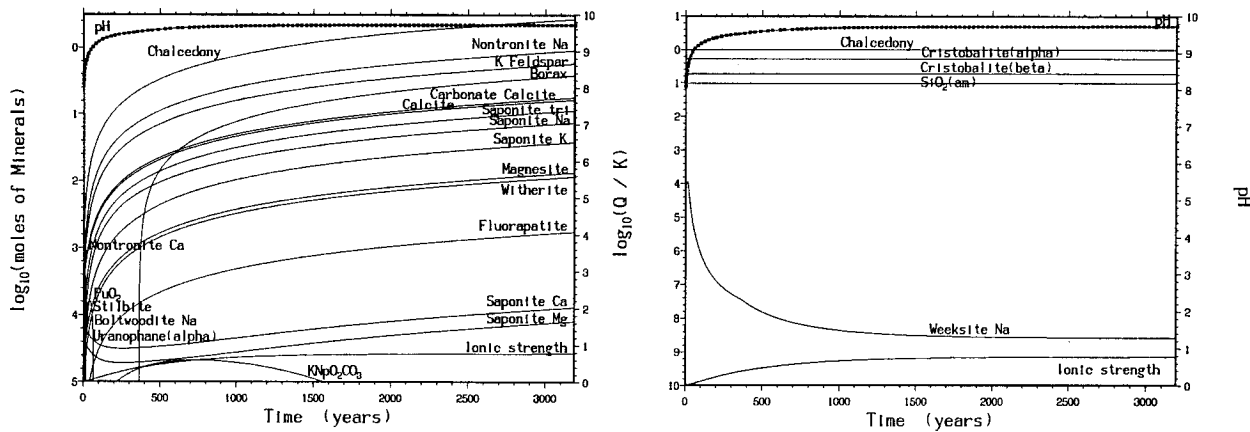


Figure 6-19: EQ6 Run with no Si Minerals Suppressed

The mineral chalcedony was suppressed first.

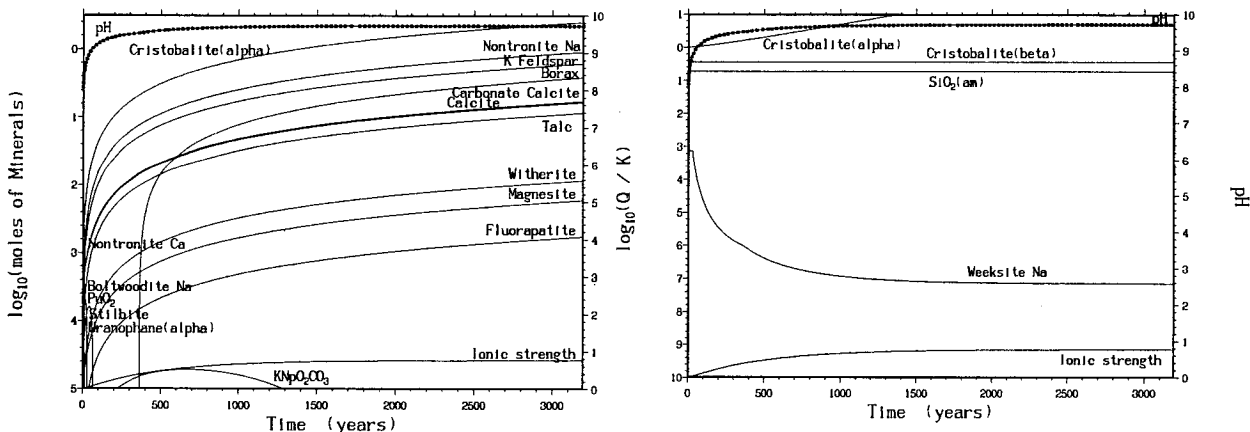


Figure 6-20: EQ6 Run with Chalcedony Suppressed

With Chalcedony suppressed, the Log(Q/K) value for weeksite at early times increases from -4 to -3, and the mineral cristobalite (alpha) formed.

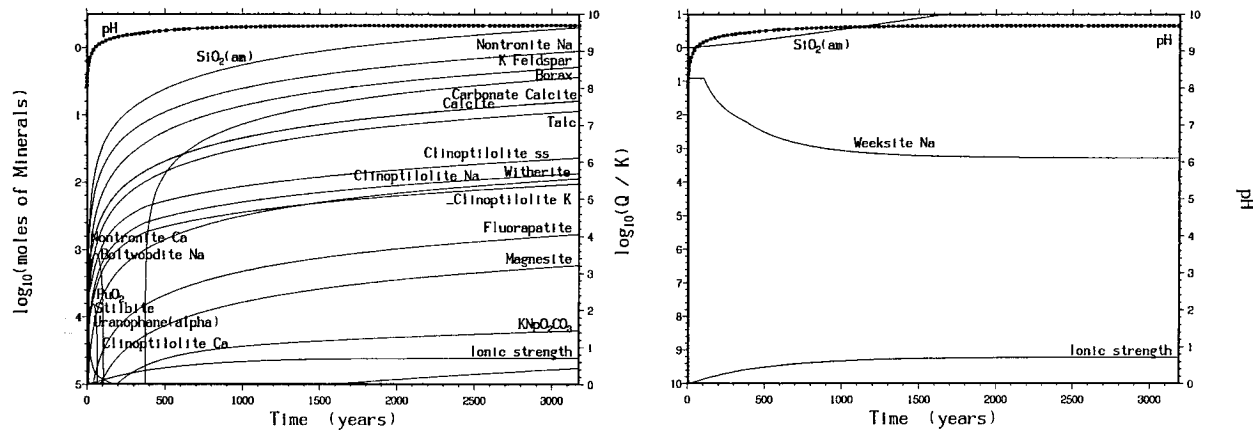


Figure 6-21: EQ6 Run with Chalcedony, Cristobalite (alpha) & (beta), and Coesite Suppressed

Suppressing two more Si minerals (cristobalite (beta) and coesite), allows the Log(Q/K) value for weeksite to jump up to -1 , but $\text{SiO}_2(\text{am})$ is still forming and taking all of the available Si.

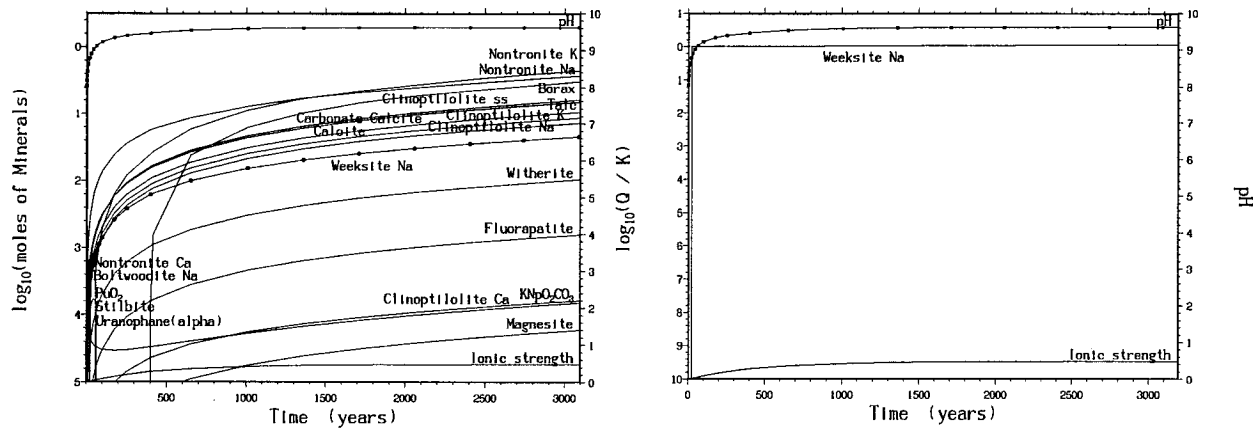


Figure 6-22: EQ6 Run with All Five Si Minerals Suppressed

Suppressing $\text{SiO}_2(\text{am})$ allows weeksite to form, and its Log(Q/K) goes to 0.

6.3.4.3 Summary

Once weeksite forms, it only stays around for the first 20,000 years while the pH is high due to the degradation of the glass. As the pH decreases with the influx of J-13, the weeksite goes back into solution.

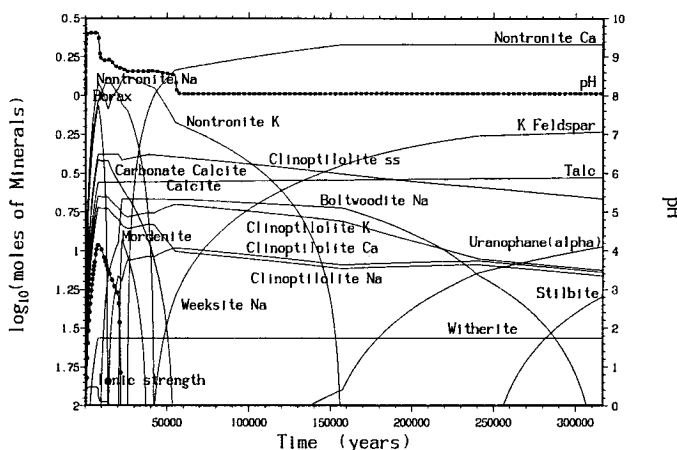


Figure 6-23: EQ6 Run with Weeksite Forming, Run out to 300,000 years

This final plot (Figure 6-23) shows the run that formed weeksite, run all the way out to 300,000 years. It is clear that weeksite forms early in the run, but then goes back into solution as the pH decreases. The minerals that were suppressed in order to form weeksite were chalcedony, cristobalite (alpha) & (beta), coesite, and $\text{SiO}_2(\text{am})$.

Uranophane was one of the other minerals observed in experimental data, and this plot shows Uranophane (alpha) forming just shy of 150,000 years. The third mineral mentioned in the experimental data, haiweeite, does not form in this run because it is no longer included in the thermodynamic database (Attachment I).

Thus, in the WP models, very high Si activity is required to make weeksite the stable alteration phase, even when steel is removed from the model. It is doubtful that such high aqueous Si would persist in a degrading WP, due to the large mass of steel corrosion products. Hence the apparent discrepancy between the U phases observed in experiments, and those predicted in the WP models, reflects the very different controls on Si activity in the two systems.

7. CONCLUSIONS

The Materials Degradation and Release Model predicts the amounts of fissile materials and neutron absorbers that remain in a WP, during an extended period of aqueous degradation. The predictions are used for evaluation of internal criticality; thus the conservatism of the model is tied to the amounts of fissile materials (Pu and U), neutron absorbers (e.g., Gd) and neutron moderators (e.g., water) that remain in the package. Implicitly, the model also predicts the compositions of the solutions that leave the WP as a function of time, to provide "source terms" for evaluation of external criticality. The model assumes a bathtub scenario, in which the WP is filled with water to a point of overflow. The model normally employs fixed fO_2 and fCO_2 , though sensitivity studies (Ref. 29 and Ref. 35) have been performed to evaluate effects of reducing conditions and redox limited by the competition between degradation and diffusion. In most calculations, the aqueous phase is assumed to be in equilibrium with all solids (corrosion products) that precipitate within the WP.

Implementation of the model was demonstrated with the examples of a Pu-ceramic WP. Degradation rates and drip rates were varied by at least two orders of magnitude. The specific combination of rates, along with the sequence of degradation were chosen to be conservative for either internal or external criticality concerns. For internal criticality, one of the most conservative cases with the highest Gd loss (s10, Table 6-8) was achieved with low steel, average glass and very high fuel (Table 6-6); whereas the most conservative for external criticality with the highest Pu discharged (case s5) was achieved with very low steel, moderately high glass, and very high fuel.

The Materials Degradation Model encompasses a large variety of combinations of glass, fuel and steel degradation rates and mechanisms; the variety of possible combinations makes it impractical to validate the model by comparison against a single analogue or lab experiment. Instead, the validation proceeds by defining the most uncertain and important sub-models; specifically, the sub-models for degradation of glass and actinide ceramics (e.g., spent fuel or Pu-ceramics). The sub-models are validated by comparison against laboratory experiments and archeological analogues.

The glass sub-model is compared against a set of MCC-4 (flow-through dissolution) experiments with an alkaline analogue of DHLW, and by comparison with a corroded archeological glass sample. The glass sub-model predicts the assemblage and approximate amounts of minerals formed in the MCC-4 tests. When kinetic precipitation is added, the sub-model also provides a reasonable prediction of the aqueous Mg concentrations. When applied to the 450-year-old archeological samples, the sub-model predicts the sequence of minerals observed in the glass-soil samples, and provides a plausible mechanism to explain why the in-soil degradation rates exceed those predicted by the MCC-4 tests.

The fuel sub-model is evaluated by comparison against the HBR-3-25 experiments of Wilson (Ref. 75) and the subsequent EQ6 calculations by Wilson and Bruton (Ref. 76). The comparison proceeds in two steps, or levels of model refinement. The first refinement reproduces the modeling of Wilson and Bruton, but takes advantage of available refinements in the thermodynamic database. However, the fundamental assumptions of the Wilson and Bruton calculation (fixed fCO_2 and fO_2) are retained. Compared to the Wilson and Bruton study, the first refinement achieves much better agreement between the observed and predicted Pu solubilities. The predicted Pu solubility is still ~20 times higher than the observed value; nonetheless, a sensitivity study shows that within this uncertainty, the Pu solubility has little

effect on the predicted performance of the WP. However, the first refinement overpredicts U solubility by about two orders of magnitude.

In the second refinement of the fuel sub-model, more realistic controls are placed on the control of fO_2 and fCO_2 , and the rate of fuel degradation is refined to be consistent with the experimental results. Consequently, the predicted and observed aqueous U concentrations match closely, and the predicted and observed Pu concentrations differ only by a factor of ~5. Given the larger uncertainties in package temperature and the ambient chemical conditions, and the uncertainty inherent in the thermodynamic database, this agreement is quite good. There is also reasonably good agreement between the predicted and observed alteration minerals.

An additional sensitivity study addresses the experimental observation that weeksite forms during the degradation of U-bearing glasses. Weeksites are not predicted in any of the WP degradation scenarios, in which actinides and glass degrade more or less simultaneously; this discrepancy suggests an inaccuracy in the degradation models. It is speculated that weeksite formation requires transient conditions of high Si activity, as might be found in a lab experiment. The sensitivity study confirms this supposition. In a WP containing abundant steel corrosion products, Si activity is likely to be controlled by the formation of Fe-rich clays, so weeksite is unlikely to provide long-term control on U solubility.

Use of the model is currently restricted, by available thermodynamic data, to temperatures of ~25 °C for actinide-bearing systems, and ≤ 100 °C for simple systems that are composed of major elements (e.g. Ca, Mg, K, Na, Fe, Si and Al). This limitation is not implicit in the model itself, and will be alleviated with future updates of the thermodynamic database. However, it is possible to approximate some temperature effects by selecting a range of rate parameters. The model is restricted to ionic strengths < 4 (preferably, ≤ 1) by use of the B-dot ionic strength correction. The model outlined in this document is restricted to "bathtub" conditions, but with minor modification, can be applied to drip-through systems (that is, systems in which the aqueous phase is not contiguous and does not fill every void within the package).

8. INPUTS AND REFERENCES

1. AP-2.21Q, Rev. 1, ICN 0, BSCN 001. *Quality Determinations and Planning for Scientific, Engineering, and Regulatory Compliance Activities*. Washington, D.C.: U.S. Department of Energy, Office of Civilian Radioactive Waste Management. ACC: MOL.20010212.0018.
2. AP-3.10Q, Rev. 2, ICN 4, ECN 1. *Analyses and Models*. Washington, D.C.: U.S. Department of Energy, Office of Civilian Radioactive Waste Management. ACC: MOL.20010827.0114.
3. AP-3.15Q, Rev. 3, ICN 0. *Managing Technical Product Inputs*. Washington, D.C.: U.S. Department of Energy, Office of Civilian Radioactive Waste Management. ACC: MOL.20010801.0318.
4. AP-SI.1Q, Rev. 3, ICN 01, ECN 02. *Software Management*. Washington, D.C.: U.S. Department of Energy, Office of Civilian Radioactive Waste Management. ACC: MOL.20010705.0239.
5. AP-SV.1Q, Rev. 0, ICN 2. *Control of the Electronic Management of Information*. Washington, D.C.: U.S. Department of Energy, Office of Civilian Radioactive Waste Management. ACC: MOL.20000831.0065.
6. ASM International 1987. *Corrosion*. Volume 13 of *ASM Handbook*. 9th Edition. Materials Park, Ohio: ASM International. TIC: 240704.
7. ASTM A 20/A20M-99a. 1999. *Standard Specification for General Requirements for Steel Plates for Pressure Vessels*. West Conshohocken, Pennsylvania: American Society of Testing and Materials. TIC: 247403.
8. ASTM A 240/A 240M-99b. 2000. *Standard Specification for Heat-Resisting Chromium and Chromium-Nickel Stainless Steel Plate, Sheet, and Strip for Pressure Vessels*. West Conshohocken, Pennsylvania: American Society for Testing and Materials. TIC: 248529.
9. ASTM A 276-91a. 1991. *Standard Specification for Stainless and Heat-Resisting Steel Bars and Shapes*. Philadelphia, Pennsylvania: American Society for Testing and Materials. TIC: 240022.
10. ASTM A 516/A 516M - 90. 1991. *Standard Specification for Pressure Vessel Plates, Carbon Steel, for Moderate- and Lower-Temperature Service*. Philadelphia, Pennsylvania: American Society for Testing and Materials. TIC: 240032.
11. ASTM G 1-90 (Reapproved 1999). 1990. *Standard Practice for Preparing, Cleaning, and Evaluating Corrosion Test Specimens*. West Conshohocken, Pennsylvania: American Society for Testing and Materials. TIC: 238771.
12. Baxter, R.G. 1988. *Defense Waste Processing Facility Wasteform and Canister Description*. DP-1606, Rev. 2. Aiken, South Carolina: E.I. du Pont de Nemours & Company, Savannah River Plant. TIC: 8704.
13. Bear, J. 1988. *Dynamics of Fluids in Porous Media*. New York, New York: Dover Publications. TIC: 217568.

14. BSC (Bechtel SAIC Company) 2001. *EQ6 Calculations for Chemical Degradation of Melt and Dilute Waste Packages*. CAL-EDC-MD-000012 REV 00. Las Vegas, Nevada: Bechtel SAIC Company. ACC: MOL.20010719.0064.
15. BSC (Bechtel SAIC Company) 2001. *EQ6 Calculation for Chemical Degradation of Pu-Ceramic Waste Packages: Effects Updated Waste Package Design and Rates*. CAL-EDC-MD-000009 REV 01. Las Vegas, Nevada: Bechtel SAIC Company. URN-0933.
16. BSC (Bechtel SAIC Company) 2001. *In-Package Chemistry for Waste Forms*. ANL-EBS-MD-000056 REV 00. Las Vegas, Nevada: Bechtel SAIC Company. ACC: MOL.20010322.0490.
17. BSC (Bechtel SAIC Company) 2001. *Technical Work Plan for: Waste Package Design Description for LA*. TWP-EBS-MD-000004 REV 01. Las Vegas, Nevada: Bechtel SAIC Company. ACC: MOL.20010702.0152.
18. BSC 2001. *Software Code: ASPRIN*. V1.0. 10487-1.0-00.
19. Cooper, G.I. and Cox, G.A. 1994. "A Comparative Study of the Natural and Experimental Corrosion of Poorly Durable Potash-Lime-Silica Glasses." *Scientific Basis for Nuclear Waste Management XVII, Symposium held November 29-December 3, 1993, Boston, Massachusetts*. Barkatt, A. and Van Konynenburg, R.A., eds. 333, 525-531. Pittsburgh, Pennsylvania: Materials Research Society. TIC: 213541.
20. Cooper, G.I. and Cox, G.A. 1996. "The Aqueous Corrosion of Potash-Lime-Silica Glass in the Range of 10–250°C." *Applied Geochemistry*, 11, ([4]), 511-521. [Oxford, England]: Elsevier. TIC: 250577.
21. Cox, G.A. and Ford, B.A. 1993. "The Long-Term Corrosion of Glass by Ground-Water." *Journal of Materials Science*, 28, (20), 5637-5647, London, England: Chapman & Hall. TIC: 245170.
22. CRWMS M&O 1996. *Second Waste Package Probabilistic Criticality Analysis: Generation and Evaluation of Internal Criticality Configurations*. BBA000000-01717-2200-00005 REV 00. Las Vegas, Nevada: CRWMS M&O. ACC: MOL.19960924.0193.
23. CRWMS M&O 1997. *Criticality Evaluation of Degraded Internal Configurations for the PWR AUCF WP Designs*. BBA000000-01717-0200-00056 REV 00. Las Vegas, Nevada: CRWMS M&O. ACC: MOL.19971231.0251.
24. CRWMS M&O 1997. *Degraded Mode Criticality Analysis of Immobilized Plutonium Waste Forms in a Geologic Repository*. Predecisional Document. A00000000-01717-5705-00014 REV 01. Las Vegas, Nevada: CRWMS M&O. ACC: MOL.19980422.0911.
25. CRWMS M&O 1998. *EQ6 Calculations for Chemical Degradation of Fast Flux Test Facility (FFTF) Waste Packages*. BBA000000-01717-0210-00028 REV 00. Las Vegas, Nevada: CRWMS M&O. ACC: MOL.19981229.0081.
26. CRWMS M&O 1998. *EQ6 Calculations for Chemical Degradation of PWR LEU and PWR MOX Spent Fuel Waste Packages*. BBA000000-01717-0210-00009 REV 00. Las Vegas, Nevada: CRWMS M&O. ACC: MOL.19980701.0483.

27. CRWMS M&O 1998. *Software Code: EQ3/6*. V7.2b. LLNL: UCRL-MA-110662.
28. CRWMS M&O 1999. *DOE SRS HLW Glass Chemical Composition*. BBA000000-01717-0210-00038 REV 00. Las Vegas, Nevada: CRWMS M&O. ACC: MOL.19990215.0397.
29. CRWMS M&O 1999. *EQ6 Calculation for Chemical Degradation of Pu-Ceramic Waste Packages: Effects of Updated Materials Composition and Rates*. CAL-EDC-MD-000003 REV 00. Las Vegas, Nevada: CRWMS M&O. ACC: MOL.19990928.0235.
30. CRWMS M&O 1999. *One (1) Compact Diskette for Electronic Data for EQ6 Calculation for Chemical Degradation of Pu-Ceramic Waste Packages: Effects of Updated Materials Composition and Rates*. CAL-EDC-MD-000003 REV 00. Las Vegas, Nevada: CRWMS M&O. ACC: MOL.19990923.0238.
31. CRWMS M&O 1999. *Software Code: EQ6, Version 7.2bLV*. V7.2bLV. 10075-7.2bLV-00.
32. CRWMS M&O 2000. *CSNF Waste Form Degradation: Summary Abstraction*. ANL-EBS-MD-000015 REV 00. Las Vegas, Nevada: CRWMS M&O. ACC: MOL.20000121.0161.
33. CRWMS M&O 2000. *Defense High Level Waste Glass Degradation*. ANL-EBS-MD-000016 REV 00. Las Vegas, Nevada: CRWMS M&O. ACC: MOL.20000329.1183.
34. CRWMS M&O 2000. *EQ6 Calculation for Chemical Degradation of Shippingport LWBR (Th/U Oxide) Spent Nuclear Fuel Waste Packages*. CAL-EDC-MD-000008 REV 00. Las Vegas, Nevada: CRWMS M&O. ACC: MOL.20000926.0295.
35. CRWMS M&O 2000. *In-Drift Accumulation of Fissile Material from Waste Packages Containing Plutonium Disposition Waste Forms*. CAL-EDC-GS-000001 REV 00. Las Vegas, Nevada: CRWMS M&O. ACC: MOL.20001016.0008.
36. CRWMS M&O 2000. *Total System Performance Assessment for the Site Recommendation*. TDR-WIS-PA-000001 REV 00 ICN 01. Las Vegas, Nevada: CRWMS M&O. ACC: MOL.20001220.0045.
37. CRWMS M&O 2000. *Unsaturated Zone Flow and Transport Model Process Model Report*. TDR-NBS-HS-000002 REV 00 ICN 02. Las Vegas, Nevada: CRWMS M&O. ACC: MOL.20000831.0280.
38. CRWMS M&O 2000. *Waste Package Degradation Process Model Report*. TDR-WIS-MD-000002 REV 00 ICN 02. Las Vegas, Nevada: CRWMS M&O. ACC: MOL.20001228.0229.
39. CRWMS M&O 2001. *Defense High Level Waste Glass Degradation*. ANL-EBS-MD-000016 REV 00 ICN 01. Las Vegas, Nevada: CRWMS M&O. ACC: MOL.20010130.0004.
40. CRWMS M&O 2001. *EQ6 Calculations for Chemical Degradation of N Reactor (U-metal) Spent Nuclear Fuel Waste Packages*. CAL-EDC-MD-000010 REV 00. Las Vegas, Nevada: CRWMS M&O. ACC: MOL.20010227.0017.
41. Deer, W.A.; Howie, R.A.; and Zussman, J. 1966. *An Introduction to the Rock-Forming Minerals*. New York, New York: John Wiley & Sons. TIC: 245492.

42. DOE (U.S. Department of Energy) 1998. *Design Specification. Volume 1 of Preliminary Design Specification for Department of Energy Standardized Spent Nuclear Fuel Canisters.* DOE/SNF/REP-011, Rev. 1. Washington, D.C.: U.S. Department of Energy, Office of Spent Fuel Management and Special Projects. TIC: 241528.

43. DOE (U.S. Department of Energy) 1998. *Total System Performance Assessment. Volume 3 of Viability Assessment of a Repository at Yucca Mountain.* DOE/RW-0508. Washington, D.C.: U.S. Department of Energy, Office of Civilian Radioactive Waste Management. ACC: MOL.19981007.0030.

44. DOE (U.S. Department of Energy) 1999. *Waste Acceptance System Requirements Document.* DOE/RW-0351, Rev. 03. Washington, D.C.: U.S. Department of Energy, Office of Civilian Radioactive Waste Management. ACC: HQO.19990226.0001.

45. DOE (U.S. Department of Energy) 2000. *Quality Assurance Requirements and Description.* DOE/RW-0333P, Rev. 10. Washington, D.C.: U.S. Department of Energy, Office of Civilian Radioactive Waste Management. ACC: MOL.20000427.0422.

46. Donnay, J.D.H. and Ondik, H.M. 1972-73. *Crystal Data: Determinative Tables.* Page C-103. Washington, DC: National Bureau of Standards. On Order Library Tracking Number-248645

47. Efurd, D.W.; Runde, W.; Banar, J.C.; Janecky, D.R.; Kaszuba, J.P.; Palmer, P.D.; Roensch, F.R.; and Tait, C.D. 1998. "Neptunium and Plutonium Solubilities in a Yucca Mountain Groundwater." *Environmental Science & Technology*, 32, (24), 3893-3900. [Easton, Pennsylvania]: American Chemical Society. TIC: 243857.

48. Eisenberg, N.A.; Lee, M.P.; Federline, M.V.; Wingefors, S.; Andersson, J.; Norrby, S.; Sagar, B.; and Wittmeyer, G.W. 1999. *Regulatory Perspectives on Model Validation in High-Level Radioactive Waste Management Programs: A Joint NRC/SKI White Paper.* NUREG-1636. Washington, D.C.: U.S. Nuclear Regulatory Commission. TIC: 246310.

49. Firsching, F.H. and Brune, S.N. 1991. "Solubility Products of the Trivalent Rare-Earth Phosphates." *Journal of Chemical Engineering*, 36, 93-95. Washington, D.C.: American Chemical Society. TIC: 240863.

50. Harrar, J.E.; Carley, J.F.; Isherwood, W.F.; and Raber, E. 1990. *Report of the Committee to Review the Use of J-13 Well Water in Nevada Nuclear Waste Storage Investigations.* UCID-21867. Livermore, California: Lawrence Livermore National Laboratory. ACC: NNA.19910131.0274.

51. Huertas, F.J.; Caballero, E.; Jimenez de Cisneros, C.; Huertas, F.; and Linares, J. 2001. "Kinetics of Montmorillonite Dissolution in Granitic Solutions." *Applied Geochemistry*, 16, (4), 397-407. New York, New York: Pergamon. TIC: 250578.

52. International Centre for Diffraction Data 1986. *Mineral Powder Diffraction File, Data Book.* Pages 16-20,28,122,172,241,269,455-456,481,491-492,535-537,770-771,787-789,792,843,861-862,966,1025-1027,1030-1032,1038-1039,1107,1193-1194. Swarthmore, Pennsylvania: International Centre for Diffraction Data. TIC: 243579.

53. Kuchment, L.S.; Demidov, V.N.; Naden, P.S.; Cooper, D.M.; and Broadhurst, P. 1996. "Rainfall-Runoff Modelling of the Ouse Basin, North Yorkshire: An Application of a Physically

Based Distributed Model." *Journal of Hydrology*, 181, (1-4), 323-342. [New York, New York]: Elsevier. TIC: 250551.

54. Latimer, W.M. 1952. *The Oxidation States of the Elements and Their Potentials in Aqueous Solutions*. 2nd Edition. Pages 8, 9, 30, 215, 270-274. New York, New York: Prentice-Hall. TIC: 238748.
55. LL000123351021.117. ANL 94/34 - The Effects of the Glass Surface Area/Solution Volume Ratio on Glass Corrosion: A Critical Review. Submittal date: 01/28/2000.
56. LLNL (Lawrence Livermore National Laboratory) 1998. *Plutonium Immobilization Project Data for Yucca Mountain Total Systems Performance Assessment, Rev. 1*. PIP 98-012. Livermore, California: Lawrence Livermore National Laboratory. ACC: MOL.19980818.0349.
57. McCright, R.D. 1998. *Corrosion Data and Modeling, Update for Viability Assessment*. Volume 3 of *Engineered Materials Characterization Report*. UCRL-ID-119564, Rev. 1.1. Livermore, California: Lawrence Livermore National Laboratory. ACC: MOL.19980806.0177.
58. MO0006J13WTRCM.000. Recommended Mean Values of Major Constituents in J-13 Well Water. Submittal date: 06/07/2000.
59. MO0009THRMODYN.001. Input Transmittal for Thermodynamic Data Input Files for Geochemical Calculations. Submittal date: 09/20/2000.
60. Mon, K. 2001. "CLST IRSR Meeting Summary." E-mail from K. Mon to [J. Nowak] (SNL), February 23, 2001, with attachment. ACC: MOL.20010328.0446.
61. Parrington, J.R.; Knox, H.D.; Breneman, S.L.; Baum, E.M.; and Feiner, F. 1996. *Nuclides and Isotopes, Chart of the Nuclides*. 15th Edition. San Jose, California: General Electric Company and KAPL, Inc. TIC: 233705.
62. Roberts, W.L.; Campbell, T.J.; and Rapp, G.R., Jr. 1990. *Encyclopedia of Minerals*. 2nd Edition. New York, New York: Van Nostrand Reinhold. TIC: 242976.
63. Shaw, H., ed. 1999. *Plutonium Immobilization Project Input for Yucca Mountain Total Systems Performance Assessment*. PIP-99-107. Livermore, California: Lawrence Livermore National Laboratory. TIC: 245437.
64. Shaw, H.F.; Ebbinghaus, B.B.; Bourcier, W.L.; and Gray, L. 2001. *Plutonium Immobilization Project Input for Yucca Mountain Total Systems Performance Assessment*. PIP-01-004, Rev. 4.0. Livermore, California: Lawrence Livermore National Laboratory. TIC: 249220.
65. SN9911T0811199.003. Calculations of Physical and Chemical Properties of Fast Flux Test Facility (FFTF) Waste Package. Submittal date: 11/15/1999.
66. Spahiu, K. and Bruno, J. 1995. *A Selected Thermodynamic Database for REE to be Used in HLNW Performance Assessment Exercises*. SKB Technical Report 95-35. Stockholm, Sweden: Swedish Nuclear Fuel and Waste Management Company. TIC: 225493.
67. Stockman, H.W. 1994. *PP: A Graphics Post-Processor for the EQ6 Reaction Path Code*. SAND94-1955. Albuquerque, New Mexico: Sandia National Laboratories. TIC: 241246.

68. Stout, R.B. and Leider, H.R., eds. 1991. *Preliminary Waste Form Characteristics Report*. Version 1.0. Livermore, California: Lawrence Livermore National Laboratory. ACC: MOL.19940726.0118.

69. Strachan, D.M.; Barnes, B.O.; and Turcotte, R.P "Standard Leach Tests for Nuclear Waste Materials." *Scientific Basis for Nuclear Waste Management, Proceedings of the Third International Symposium*, Boston, Massachusetts, November 17-20, 1980. Moore, J.G., ed. 3, 347-354. New York, New York: Plenum Press. TIC: 204407.

70. Towe, K.M. and Bradley, W.F. 1967. "Mineralogical Constitution of Colloidal 'Hydrous Ferric Oxides'." *Journal of Colloid and Interface Science*, 24, 384-392. [New York, New York: Academic Press]. TIC: 250230.

71. Turner, D.R. and Pabalan, R.T. 1999. "Abstraction of Mechanistic Sorption Model Results for Performance Assessment Calculations at Yucca Mountain, Nevada." *Waste Management*, 19, (6), 375-388. New York, New York: Pergamon Press. TIC: 246704.

72. Vernaz, E. Y. and Godon, N. 1991. "Key Parameters of Glass Dissolution in Integrated Systems." *Scientific Basis for Nuclear Waste Management XIV, Symposium held November 26-29, 1990, Boston, Massachusetts*, Abrajano, T. A., Jr. and Johnson, L.H., eds. 212, 19-30. Pittsburgh, Pennsylvania: Materials Research Society. TIC: 203656.

73. Weast, R.C. and Astle, M.J., eds. 1979. *CRC Handbook of Chemistry and Physics*. 60th Edition. 2nd Printing 1980. Boca Raton, Florida: CRC Press. TIC: 245312.

74. Weast, R.C., ed. 1977. *CRC Handbook of Chemistry and Physics*. 58th Edition. Cleveland, Ohio: CRC Press. TIC: 242376.

75. Wilson, C.N. 1988. "Summary of Results from the Series 2 and Series 3 NNWSI Bare Fuel Dissolution Tests." *Scientific Basis for Nuclear Waste Management XI, Symposium held November 30-December 3, 1987, Boston, Massachusetts*. Apted, M.J. and Westerman, R.E., eds. 112, 473-483. Pittsburgh, Pennsylvania: Materials Research Society. TIC: 203662.

76. Wilson, C.N. and Bruton, C.J. 1989. *Studies on Spent Fuel Dissolution Behavior Under Yucca Mountain Repository Conditions*. PNL-SA-16832. Richland, Washington: Pacific Northwest Laboratory. ACC: HQX.19890918.0047.

77. Wolery, T.J. and Daveler, S.A. 1992. *EQ6, A Computer Program for Reaction Path Modeling of Aqueous Geochemical Systems: Theoretical Manual, User's Guide, and Related Documentation (Version 7.0)*. UCRL-MA-110662 PT IV. Livermore, California: Lawrence Livermore National Laboratory. TIC: 205002.

78. Yang, I.C.; Rattray, G.W.; and Yu, P. 1996. *Interpretation of Chemical and Isotopic Data from Boreholes in the Unsaturated Zone at Yucca Mountain, Nevada*. Water-Resources Investigations Report 96-4058. Denver, Colorado: U.S. Geological Survey. ACC: MOL.19980528.0216.

9. ATTACHMENTS

- I. One Compact Disk (CD) containing the EQ3/6 computer files and Excel spreadsheets.
- II. Listing of Files on Compact Disk, 5 pages.
- III. Sketch SK-0196 Rev. 3, 5 DHLW/DOE -WP Assembly Configuration for Site Recommendation, 2 pages.

Attachment II. Listing of Files on Compact Disk

This attachment contains the MS-DOS directory for files placed on the electronic media (Attachment I). The files are of various types:

1. Excel files (extensions = xls).

2. EQ3/6 input files (extension = 3i or 6i).

ASCII text file: provides input parameters for EQ3/6.

3. EQ3/6 output files (extension = 3o or 6o).

ASCII text file: provides detailed information about the system at each print point, which is specified by the user in the input file.

4. EQ3/6 pickup files (extension = 3p or 6p).

ASCII text file: provides a description of the system at the end of that run to be used as an input file for a continuation run.

5. EQ6 Tab-delimited text files (extension = txt).

*.elem_aqu: total aqueous moles of elements.

*.elem_min: total moles of elements in minerals.

*.elem_tot: total moles of elements (aqueous + mineral).

*.min_info: moles of each mineral.

6. EQ6 binary output file (extension = bin).

Binary file: provides detailed information about the system at the full numerical precision for *every* time step.

7. EQ3/6 text data files used for the calculations, located in folder "databases", with name 'data0.yme'.

8. Batch files (extension = bat) used to start EQ6 runs.

9. Winzip files (extension = zip).

Below are listed the contents of the DOS directories within the electronic attachment:

The first column is the DOS file name.

The second column lists <DIR> if it is a directory
or gives the files size (bytes) if it is a file.

The third and fourth columns are the date and time of the last update.

The fifth column is the filename.

Directory of Disk

DOS FILE NAME	SIZE (IF A FILE)	DATE	TIME	FILE NAME
DATABA~5	<DIR>	09-07-01	11:45a	databases
FUEL2	<DIR>	09-07-01	11:07a	Fuel2
GLASS	<DIR>	09-07-01	11:08a	Glass
J13WSF	<DIR>	09-07-01	11:09a	j13wsf
MINERALS	<DIR>	09-07-01	11:05a	Minerals
PU199~15	<DIR>	09-07-01	11:45a	Pu 1999
PU200~17	<DIR>	09-07-01	11:45a	Pu 2001
	0 file(s)		0 bytes	

Directory of F:\databases

DATA0	YME	2,658,654	08-27-01	11:39a	data0.yme
		1 file(s)			2,658,654 bytes

Directory of F:\Fuel2

(Files used in Section 6.3.2.2)

ELEM_AQU BIN	13,964	08-23-01	11:46a	elem_aqu.bin
ELEM_AQU TXT	22,401	08-23-01	11:46a	elem_aqu.txt
ELEM_M_A TXT	21,216	08-23-01	11:46a	elem_m_a.txt
ELEM_MIN TXT	21,208	08-23-01	11:46a	elem_min.txt
ELEM_TOT TXT	21,221	08-23-01	11:46a	elem_tot.txt
J13FU~18 XLS	39,424	08-28-01	1:32p	j13fuel_081001.xls
J13SFUEL 6I	30,791	08-23-01	11:34a	j13sfuel.6i
J13SF~22 6O	2,050,574	08-23-01	11:46a	j13sfuel.6i.6o
J13SF~30 6P	33,453	08-23-01	11:46a	j13sfuel.6i.6p
J13SF~32 6T	218,400	08-23-01	11:46a	j13sfuel.6i.6t
J13SF~36 6TX	122,906	08-23-01	11:46a	j13sfuel.6i.6tx
J13SFUEL BIN	7,893,328	08-23-01	11:46a	J13SFUEL.BIN
J13SFUEL TX0	46,731	08-27-01	8:54a	J13SFUEL.TX0
MIN_INFO TXT	42,566	08-23-01	11:46a	min_info.txt
	15 file(s)			10,578,813 bytes

Directory of F:\Glass

(Files used in Section 6.3.1)

CLAY!H2O 6I	24,764	08-20-01	10:50a	clay!H2o.6i
CLAY_H2O 3I	8,690	08-15-01	8:36a	clay_h2o.3i
CLAY_H2O 6I	24,689	08-15-01	8:41a	clay_H2o.6i
ELEM_~14 XLS	176,128	08-31-01	6:57a	elem_Stain00a_staine6a_stai_e6s.xls
GLA!CLY0 6I	25,345	08-23-01	8:51a	gla!cly0.6i
GLA!CLY1 6I	25,641	08-20-01	2:28p	gla!cly1.6i
GLA!CLY2 6I	25,614	08-20-01	1:50p	gla!cly2.6i
GLA!CLY3 6I	25,762	08-20-01	2:50p	gla!cly3.6i
GLASCLY0 6I	25,158	08-15-01	4:45p	glasclly0.6i
GLASCLY1 6I	25,454	08-20-01	1:27p	glasclly1.6i
GLASCLY2 6I	25,649	08-20-01	1:27p	glasclly2.6i
GLASCLY3 6I	25,723	08-20-01	1:27p	glasclly3.6i
GLASS~32 XLS	55,296	08-31-01	6:57a	glass_archeol.xls
MG_ST~34 XLS	71,680	08-31-01	6:57a	Mg_stain_glass_expt.xls
STAI!E6S 6I	27,485	08-13-01	7:44p	stai!e6S.6i
STAI_E6S 6I	27,631	08-22-01	6:26p	stai_e6s.6i
STAIN00 3I	8,644	08-02-01	4:46p	stain00.3i
STAIN00A 6I	25,118	08-22-01	6:26p	stain00A.6i
STAIN00B 6I	24,647	08-02-01	9:46p	stain00B.6i
STAIN01! 6I	24,504	08-03-01	8:18p	stain01!.6i
STAIN01A 6I	24,390	08-20-01	5:14p	stain01A.6i
STAIN1A 6I	24,538	08-13-01	1:28p	stain1A.6i

STAINE2A 6I	24,612	08-13-01	1:54p	staine2A.6i
STAINE3A 6I	24,612	08-13-01	1:57p	staine3A.6i
STAINE4A 6I	24,612	08-13-01	2:07p	staine4A.6i
STAINE5A 6I	24,612	08-13-01	2:11p	staine5A.6i
STAINE6A 6I	24,612	08-13-01	2:22p	staine6A.6i
STAINE6S 6I	27,408	08-13-01	6:03p	staine6S.6i

28 file(s) 903,018 bytes

Directory of F:\j13wsf

(Files used in Section 6.3.2.1)

DECAYE~6 241	10	01-25-00	11:23a	decay.eq6.24100
J13WSF13 6I	28,648	08-28-01	2:25p	j13wsf13.6i
J13WSF13 6O	1,121,844	08-28-01	2:30p	j13wsf13.6o
J13WSF13 6P	30,441	08-28-01	2:30p	j13wsf13.6p
J13WSF13 6T	74,563	08-28-01	2:30p	j13wsf13.6t
J13WSF13 6TX	75,681	08-28-01	2:30p	j13wsf13.6tx
J13WSF13 BAT	371	08-28-01	2:26p	j13wsf13.bat
J13WSF13 BIN	3,102,800	08-28-01	2:30p	j13wsf13.bin
J13WS~34 TXT	18,436	08-28-01	2:30p	j13wsf13.elem_aqu.txt
J13WS~36 TXT	17,507	08-28-01	2:30p	j13wsf13.elem_min.txt
J13WS~38 TXT	17,520	08-28-01	2:30p	j13wsf13.elem_tot.txt
J13WS~40 TXT	27,265	08-28-01	2:30p	j13wsf13.min_info.txt
J13WSF_ 6I	28,499	08-04-99	7:57p	j13wsf_.6i
J13WSF_ 6O	1,105,389	07-20-01	11:50a	j13wsf_.6o
J13WSF_ 6P	30,099	07-20-01	11:50a	j13wsf_.6p
J13WSF_ 6T	72,919	07-20-01	11:50a	j13wsf_.6t
J13WSF_ 6TX	74,020	07-20-01	11:50a	j13wsf_.6tx
J13WSF_ BAT	365	07-20-01	11:46a	j13wsf_.bat
J13WSF_ BIN	3,093,008	07-20-01	11:50a	j13wsf_.bin
J13WS~70 TXT	17,967	07-20-01	11:50a	j13wsf_.elem_aqu.txt
J13WS~72 TXT	17,062	07-20-01	11:50a	j13wsf_.elem_min.txt
J13WS~74 TXT	17,075	07-20-01	11:50a	j13wsf_.elem_tot.txt
J13WS~76 TXT	26,517	07-20-01	11:50a	j13wsf_.min_info.txt
J13WSF_ XLS	180,736	08-30-01	2:31p	J13WSF_.xls
P52L1~80 XLS	74,752	08-29-01	9:54a	p52_L142.loss.xls
P52_L142 6I	44,420	08-28-01	4:00p	p52_L142.6i
P52_L142 6O	9,348,863	08-28-01	4:44p	p52_L142.6o
P52_L142 BAT	541	08-28-01	3:01p	P52_L142.bat
P52_L142 BIN	111,585,016	08-28-01	4:44p	p52_L142.bin
P52_~444 TXT	85,121	08-28-01	4:44p	p52_L142.elem_aqu.txt
P52_~446 TXT	79,992	08-28-01	4:44p	p52_L142.elem_min.txt
P52_~448 TXT	80,005	08-28-01	4:44p	p52_L142.elem_tot.txt
P52_~450 TXT	179,352	08-28-01	4:44p	p52_L142.min_info.txt
P52AL142 6I	44,568	08-28-01	4:02p	p52al142.6i
P52AL142 6O	9,360,237	08-28-01	5:26p	p52al142.6o
P52AL142 BIN	111,553,840	08-28-01	5:26p	p52al142.bin
P52A~814 TXT	85,518	08-28-01	5:26p	p52al142.elem_aqu.txt
P52A~818 TXT	80,365	08-28-01	5:26p	p52al142.elem_min.txt
P52A~820 TXT	80,378	08-28-01	5:26p	p52al142.elem_tot.txt
P52A~822 TXT	180,136	08-28-01	5:26p	p52al142.min_info.txt

40 file(s) 252,041,846 bytes

Directory of F:\Minerals

(Files used in Section 6.3.3)

F_1_0522 6I	35,958	08-10-01	9:47a	f_1_0522.6i
F_1_05~8 6O	943,588	09-04-01	4:50p	f_1_0522.6i.6o
F_1_0~12 6P	32,654	09-04-01	4:50p	f_1_0522.6i.6p
F_1_0~14 6T	106,340	09-04-01	4:50p	f_1_0522.6i.6t
F_1_0~18 6TX	57,117	09-04-01	4:50p	f_1_0522.6i.6tx
F_1_0~20 ELE	9,121	09-04-01	4:50p	f_1_0522.6i.elem_aqu
F_1_0~22 ELE	8,560	09-04-01	4:50p	f_1_0522.6i.elem_m_a
F_1_0~24 ELE	8,552	09-04-01	4:50p	f_1_0522.6i.elem_min
F_1_0~26 ELE	8,565	09-04-01	4:50p	f_1_0522.6i.elem_tot
F_1A0522 6I	36,031	08-10-01	9:48a	f_1a0522.6i
F_1A0~30 6O	885,386	09-04-01	4:52p	f_1a0522.6i.6o
F_1A0~34 6P	32,564	09-04-01	4:52p	f_1a0522.6i.6p
F_1A0~36 6T	95,420	09-04-01	4:52p	f_1a0522.6i.6t
F_1A0~40 6TX	50,522	09-04-01	4:52p	f_1a0522.6i.6tx
F_1A0~42 ELE	8,748	09-04-01	4:52p	f_1a0522.6i.elem_aqu
F_1A0~44 ELE	8,211	09-04-01	4:52p	f_1a0522.6i.elem_m_a
F_1A0~46 ELE	8,203	09-04-01	4:52p	f_1a0522.6i.elem_min
F_1A0~48 ELE	8,216	09-04-01	4:52p	f_1a0522.6i.elem_tot
F_1B0522 6I	36,030	08-10-01	9:48a	f_1b0522.6i
F_1B0~52 6O	879,433	09-04-01	4:54p	f_1b0522.6i.6o
F_1B0~56 6P	32,638	09-04-01	4:54p	f_1b0522.6i.6p
F_1B0~58 6T	95,420	09-04-01	4:54p	f_1b0522.6i.6t
F_1B0~60 6TX	50,522	09-04-01	4:54p	f_1b0522.6i.6tx
F_1B0~62 ELE	8,748	09-04-01	4:54p	f_1b0522.6i.elem_aqu
F_1B0~64 ELE	8,211	09-04-01	4:54p	f_1b0522.6i.elem_m_a
F_1B0~66 ELE	8,203	09-04-01	4:54p	f_1b0522.6i.elem_min
F_1B0~68 ELE	8,216	09-04-01	4:54p	f_1b0522.6i.elem_tot
F_1C0522 6I	36,104	08-10-01	10:54a	f_1c0522.6i
F_1C0~72 6O	907,705	09-04-01	4:56p	f_1c0522.6i.6o
F_1C0~78 6P	32,712	09-04-01	4:56p	f_1c0522.6i.6p
F_1C0~80 6T	97,890	09-04-01	4:56p	f_1c0522.6i.6t
F_1C0~82 6TX	51,921	09-04-01	4:56p	f_1c0522.6i.6tx
F_1C0~84 ELE	9,121	09-04-01	4:56p	f_1c0522.6i.elem_aqu
F_1C0~86 ELE	8,560	09-04-01	4:56p	f_1c0522.6i.elem_m_a
F_1C0~88 ELE	8,552	09-04-01	4:56p	f_1c0522.6i.elem_min
F_1C0~90 ELE	8,565	09-04-01	4:56p	f_1c0522.6i.elem_tot
F_1D0522 6I	36,177	08-10-01	11:00a	f_1d0522.6i
F_1D0~94 6O	921,115	09-04-01	4:57p	f_1d0522.6i.6o
F_1D0~98 6P	33,360	09-04-01	4:57p	f_1d0522.6i.6p
F_1D~100 6T	103,870	09-04-01	4:57p	f_1d0522.6i.6t
F_1D~104 6TX	55,156	09-04-01	4:57p	f_1d0522.6i.6tx
F_1D~106 ELE	9,121	09-04-01	4:57p	f_1d0522.6i.elem_aqu
F_1D~108 ELE	8,560	09-04-01	4:57p	f_1d0522.6i.elem_m_a
F_1D~110 ELE	8,552	09-04-01	4:57p	f_1d0522.6i.elem_min
F_1D~112 ELE	8,565	09-04-01	4:57p	f_1d0522.6i.elem_tot
F_1E0522 6I	36,176	08-10-01	11:08a	f_1e0522.6i
F_1E~116 6O	4,222,609	09-04-01	5:04p	f_1e0522.6i.6o
F_1E~130 6P	33,188	09-04-01	5:04p	f_1e0522.6i.6p
F_1E~132 6T	291,590	09-04-01	5:04p	f_1e0522.6i.6t
F_1E~134 6TX	179,156	09-04-01	5:04p	f_1e0522.6i.6tx
F_1E~138 ELE	36,350	09-04-01	5:04p	f_1e0522.6i.elem_aqu
F_1E~140 ELE	34,037	09-04-01	5:04p	f_1e0522.6i.elem_m_a
F_1E~142 ELE	34,029	09-04-01	5:04p	f_1e0522.6i.elem_min
F_1E~144 ELE	34,042	09-04-01	5:04p	f_1e0522.6i.elem_tot
FFTF~146 XLS	44,032	09-05-01	9:56a	FFTF IA 2001.xls
FFTF~148 XLS	955,904	08-06-01	4:05p	fftf_fuel_hws_rev4.xls

56 file(s) 11,717,896 bytes

Directory of F:\Pu 1999

(Files used in Section 6.3.2.1; the source is Ref. 40.)

PU-CERAM XLS	922,624	09-12-99	4:36p	pu-ceram.xls
1 file(s)	922,624	bytes		

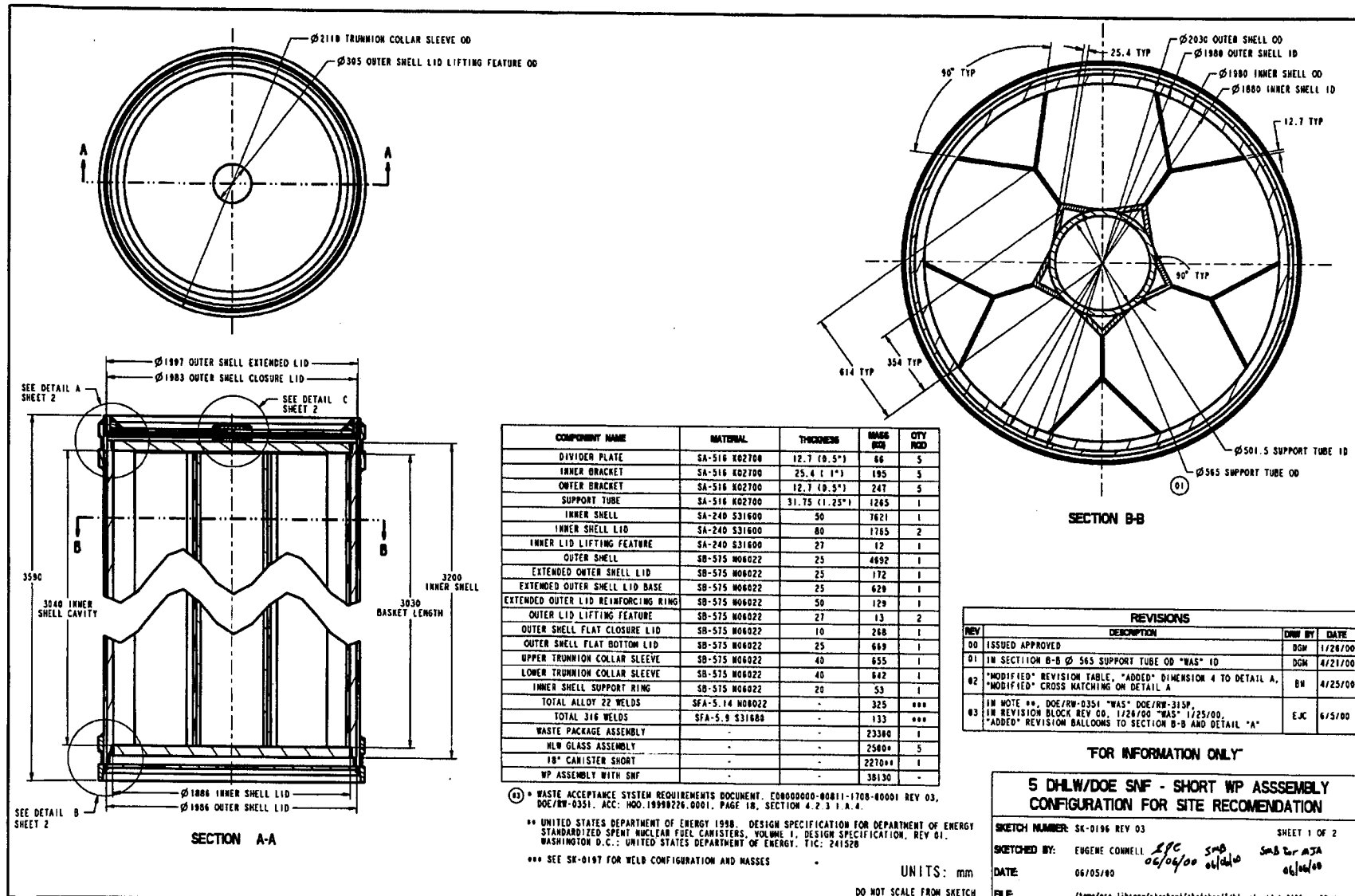
Directory of F:\Pu 2001

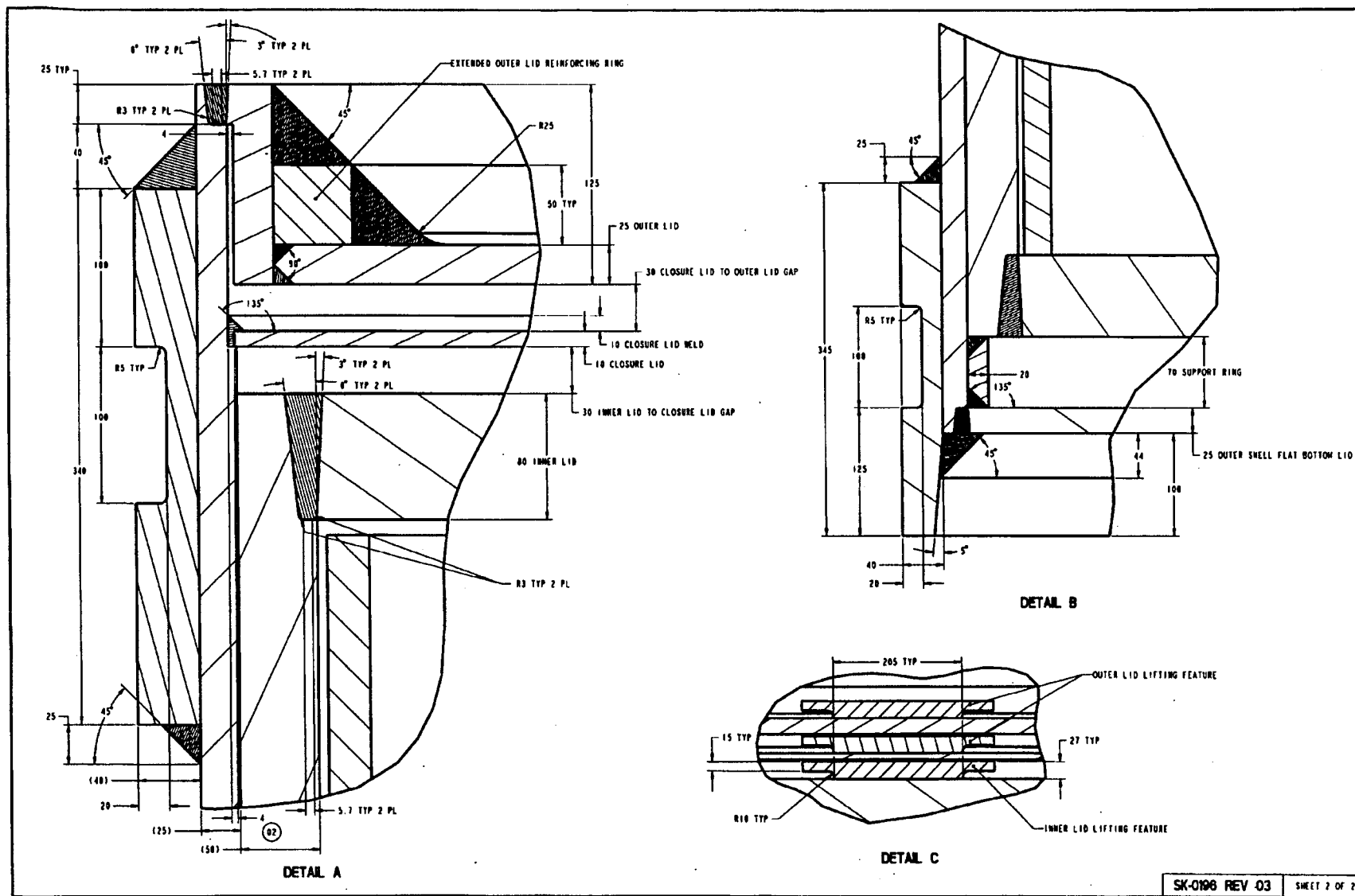
(Files used in Section 6.3.2.1; the source is Ref. 18.)

A516_R~6 XLS	19,456	01-20-01	5:23p	A516_Rate.xls
DENSIT~8 XLS	274,944	08-27-01	4:12p	density_pu-ceram.xls
HLW_G~10 XLS	58,368	08-17-01	1:26p	HLW_glass REV01.xls
SLEEVE XLS	15,360	02-06-01	1:59p	Sleeve.xls
4 file(s)	368,128	bytes		

Total files listed:

145 file(s) 279,190,979 bytes





OFFICE OF CIVILIAN RADIOACTIVE WASTE MANAGEMENT
SPECIAL INSTRUCTION SHEET
Complete Only Applicable Items

1. QA: QA
Page: 1 of 1

file list
10-17-01

MFC

This is a placeholder page for records that cannot be scanned.

2. Record Date 09/28/2001	3. Accession Number <i>ATT-TO MOL 20011017.0091</i>
4. Author Name(s) SUSAN LESTRANGE	5. Author Organization N/A
6. Title/Description GEOCHEMISTRY MODEL VALIDATION REPORT: MATERIAL DEGRADATION AND RELEASE MODEL	
7. Document Number(s) ANL-EBS-GS-000001	8. Version Designator REV. 00
9. Document Type DATA	10. Medium CD-ROM
11. Access Control Code PUB	
12. Traceability Designator DC# 28774	<i>10-18-01 (AB)</i>
13. Comments THIS IS A SPECIAL PROCESS CD-ROM AS PART OF ATTACHMENT I AND CAN BE LOCATED THROUGH THE RPC.	

THIS DATA SUBMITTAL TO THE
RECORDS PROCESSING CENTER IS
FOR ARCHIVE PURPOSES ONLY, AND
IS NOT AVAILABLE FOR VIEWING OR
REPRODUCTION

1082

OFFICE OF CIVILIAN RADIOACTIVE WASTE MANAGEMENT
ELECTRONIC FILE CERTIFICATION

QA: N/A

1. DOCUMENT TITLE:

Geochemistry Model Validation Report: Material Degradation and Release Model

2. IDENTIFIER (e.g., DI OR PI):

ANL-EBS-GS-000001

3. REVISION DESIGNATOR:

Rev. 00

ATTACHED SOFTWARE FILE INFORMATION

4. PDF FILE SUBMITTED:

YES

NO

5. FILE NAMES(S) WITH FILE EXTENSION(S) PROVIDED BY THE SOFTWARE:

See Attached

6. DATE LAST MODIFIED:

See Attached

7. NATIVE APPLICATION:

(i.e., EXCEL, WORD, CORELDRAW)

Word, Excel, pp.exe

8. FILE SIZE IN KILOBYTES:

See Attached

9. FILE LINKAGE INSTRUCTIONS/INFORMATION:

Standard

10. PRINTER SPECIFICATION (I.E., HP4SI) INCLUDING POSTSCRIPT INFORMATION (i.e., PRINTER DRIVER) AND PRINTING PAGE SETUP: (i.e., LANDSCAPE, 11 X 17 PAPER)

8 1/2 x 11(Potrait & Landscape)- Hewlett Packard LaserJet 5s: / color T1005 HP5 MC

11. COMPUTING PLATFORM USED: (i.e., PC, SUN, WIN 95, NT, HP)

PC#115815

12. OPERATING SYSTEM AND VERSION: (i.e., WINDOWS UNIX, SOLARIS)

Windows

13. ADDITIONAL HARDWARE/SOFTWARE REQUIREMENT USED TO CREATE FILE(S):

None

14. ACCESS RESTRICTIONS: (COPYRIGHT OR LICENSE ISSUES)

None

COMMENTS/SPECIAL INSTRUCTIONS

15. IS SOFTWARE AVAILABLE FROM SOFTWARE CONFIGURATION MANAGEMENT? YES NO
 SOFTWARE MEDIA TRACKING NUMBER N/A

NOTE: The software product(s) to develop this document are Commercial-Off-The-Shelf (COTS) software products which require no Software Media Number (SMN). The COTS software products are under Software Configuration Management (SCM) control.

CERTIFICATION

16. DOCUMENT OWNER (Print and Sign):

Susan LeStrange

Susan LeStrange

17. DATE:

10/01/2001

18. ORGANIZATION:

BSC

19. DEPARTMENT:

Waste Package

20. LOCATION/MAIL STOP:

MS423/1028F

21. PHONE:

295-4580

22. SUBMITTED BY (Print and Sign):

Dnyett D Vosicky Dnyett D. Vosicky

10-4-2001

DC USE ONLY

24. DATE RECEIVED:

10-4-01

25. DATE FILES TRANSFERRED:

n/a

26. DC NO.:

28774

27. NAME (Print and Sign):

n/a

28. DATE:

10-4-01

U

Name	Size	Type	Modified
databases		File Folder	09/07/2001 11:45 AM
Fuel2		File Folder	09/07/2001 11:07 AM
Glass		File Folder	09/07/2001 11:08 AM
j13wsf		File Folder	09/07/2001 11:09 AM
Minerals		File Folder	09/07/2001 11:05 AM
Pu 1999		File Folder	09/07/2001 11:45 AM
Pu 2001		File Folder	09/07/2001 11:45 AM

7 object(s)

50.0KB